るというものまで様々な説があり、決着がついていない。移植片にレビー小体ができるからといって、その細胞が障害されるとは限らないのである。

また、移植後10年以上を経ないとレビー小体形成は見られないことから、たとえレビー小体に毒性があったとしても10年以内の効果は十分望みうることになる。胎児黒質移植自体は2件の二重盲検試験で有意な症状の改善効果がなく、多彩な不随意運動が生じるなどの副作用があることが示され、現在中われていないが、広く移植治療の一つものは方法論の改善で有用段階療法になる可能性は秘めてお

そのような意味で、今後も新1)な治療の選択肢として研究を続けるべきと思われる。

神経新生の治療に関しても同様の理由で、Nature Medicineの論文の結果が、治療法そのものを否定することにはならない。動物実験ではあるが、海馬における神経新生が抗うつ薬の効果発現に必須であることが示された[5]。これは、神経新生治療がパーキンソン病を含めた様々な神経疾患でも有用であることを強く示唆している。

パーキンソン病でも黒質ドーパミン神経の新生を示唆する報告があり、期待が持たれる[6]。ただし、一方でレビー小体が移植細胞、新生した細胞に生じた場合、それが細胞機能に与える影響を正確に評価する研究も進め、移植治療、神経新生治療の可能性と限界を明らかにすることが、これらの治療を将来的に現実のものとする上で重要であろう。

文　献

1) Li JY, et al : Nature Med 14 : 501, 2008.
2) Kordower JH, et al : Nature Med 14 : 504, 2008.
3) Mendez I, et al : Nature Med 14 : 507, 2008.
4) Brundin P, et al : Nat Rev Neurosci 9 : 741, 2008.
5) Santarelli L, et al : Science 301 : 805, 2003.
6) Yoshimi K, et al : Ann Neurol 58 : 31, 2005.

京都大学医学研究科臨床神経学
（神経内科）教授
高橋良輔

赤痢アメーバ症の診断と治療

Q

赤痢アメーバ症の診断と治療について、以下を。

(1)糞便検体の採取方法（顕微鏡検査用、培養検査用）。

(2)血液検査用の検体採取方法（検査名、検査結果の判読）。

(3)治療方法、治療期間。

(4)治療効果の確認方法。

（東京都　M）

A

糞便の顕微鏡検査で赤痢アメーバの嚢子あるいは栄養型に一致する形態を確認しても、赤痢アメーバ（*Entamoeba histolytica*）と報告してはならない。赤痢アメーバないしは非病原性のアメーバ（*E. histolytica*/*E. dispar*, 以下Eh/Edと略）と報告すべきである。赤痢アメーバ症を疑わせる症状がある場合、Eh/Edの検出をもって治療適応となる。健康人から検出されたEh/Edは治療適応とならない[1]。

(1)結果報告書に赤痢アメーバと記述できるのは、赤痢アメーバに特異的な検査を実施した場合のみである。赤痢アメーバの検査は国立感染症研究所あるいは地方衛生研究所で実施可能である[2]。検体採取法はそちらの指示に従っていただきたい。

自らの手で確認したい場合は、赤痢アメーバ抗原検出キットであるE. HISTOLYTICA II（関東科学から購入可）を入手すればよい。ただし、これは正式な検査法として認められていない。このため、法律上「診断に用いてはならない」ことになっている。

(2)アメーバ性肝膿瘍では、必ずしも糞便中に赤痢アメーバが検出できるとは限らない。血中抗赤痢アメーバ抗体の検出をもって、抗アメーバ薬の適否を判断する場合が多い。詳細は、参考文献をご覧いただきたい[2]。

(3)治療方法

第1選択薬はメトロニダゾールの経口投与である。海外の文献では2250mg／日の記述もみられるが、日本人には、1500mg分3、10日間で十分である[3]。なお、

Experimental Neurology 217 (2009) 235–236

Contents lists available at ScienceDirect

Experimental Neurology

journal homepage: www.elsevier.com/locate/yexnr

Commentary

Edaravone in ALS

Ryosuke Takahashi

Department of Neurology, Kyoto University Graduate School of Medicine, 54 Shogoin-Kawaharacho, Sakyoku, Kyoto 606-8507, Japan

ARTICLE INFO

Article history:
Received 30 December 2008
Revised 28 February 2009
Accepted 3 March 2009
Available online 10 March 2009

Amyotrophic lateral sclerosis (ALS) is a devastating neurodegenerative disorder characterized by progressive and relatively selective degeneration of upper and lower motor neurons. Patients suffer from atrophy and paralysis of systemic voluntary muscles including respiratory muscles, leading to respiratory failure and subsequent death 3–5 years after the disease onset. Effective therapy for ALS that ameliorates its clinical course is still not known (Mitchell and Borasio, 2007).

Although ALS usually develops sporadically, 5 to 10% of cases are familial and hereditary. Twenty percent of familial ALS (FALS) are caused by mutations in the *copper and zinc-dependent superoxide dismutase* (*SOD1*) gene, which was first reported in 1993 (Rosen et al., 1993). Mutant SOD1 brought a breakthrough to this field, since mutant SOD1 transgenic mice recapitulate the clinical symptoms and pathological findings of human FALS (Gurney et al., 1994). Mutant SOD1 transgenic mouse models provided invaluable tools for testing effective drugs which extend their lifespan. Up to now, more than 20 drugs have been claimed to be effective in the therapy of mouse ALS.

A big problem, however, is arising: none of these drugs have yet to be shown to be effective as well in human sporadic ALS (SALS) patients (Benatar, 2007). Why? A couple of explanations are conceivable. First, mutant SOD1 transgenic mice may not be a good model for human sporadic ALS cases despite their apparent similarities. Indeed, mutant SOD1 associated FALS and SALS exhibit different microscopic neuropathology. The former is characterized by Lewy body-like inclusion containing mutant SOD1, whereas for the latter skein-like or round inclusions containing TDP-43. Since TDP-43 is implicated in the pathogenesis of SALS as well as in a subgroup of FALS, developing a new ALS mouse model based on TDP-43 could solve these problems in the future (Neumann et al., 2007). A second possible explanation is that the most therapies in mouse models are initiated prior to disease onset, which is impossible in human patients until presymptomatic diagnosis for ALS becomes available. Thirdly, whether drug dosage and bioavailablity comparable to mouse experiments are replicated in human trials remains unclear.

An alternative explanation is the difference in the design of mouse experimental therapies and human clinical trials. Randomized controlled trials, which are designed to eliminate numerous confounding factors including observation biases, are standard in human clinical trials. In contrast, mouse experiments are generally not performed as rigorously as human trials, increasing risks of producing "false positive" results (Benatar, 2007).

Edaravone (3-methyl-1-phenyl-2-pyrazolin-5-one) is a free radical scavenger that has been approved in Japan since 2001 as a therapeutic agent to reduce neuronal damage caused by acute ischemic stroke (Yoshida et al., 2006). Edaravone eliminates lipid peroxide and hydroxyl radicals by transferring an electron to the radical, thereby ameliorating the ischemic neuronal damage. Oxidative stress is implicated as one of the pathogenetic mechanisms for ALS (Barber et al., 2006). Moreover, a small-sized open trial of edaravone suggested that edaravone is safe and may delay the progression of functional motor disturbances in ALS patients (Yoshino and Kimura, 2006). Thus, edaravone is a promising therapeutic agent for human motor neuron diseases including ALS.

In a previous issue, Ito et al. reported an experimental therapy of a mutant SOD1 mouse model using edaravone (Ito et al., 2008). Taking the problems associated with the therapeutic experimental design in mouse experiments, they carefully optimized the dosage of edaravone so that the pharmacokinetic profile after intraperitoneal injection became comparable to that in human patients. Moreover, they started treatment only after the disease onset, similar to human ALS treatment. Furthermore, they used only female mice for analysis considering the gender difference in lifespan and randomized blind analyses were adopted for all the behavioral as well as pathological observations. This methodological rigorousness has never been considered seriously in previous experimental therapies of mutant SOD1 ALS mouse models, most of which have failed to be replicated in human patients.

Edaravone significantly slowed the motor function decline as assessed by multiple behavioral tests such as rotarod tests. However, the lifespan of edaravone-treated mice were not significantly higher

Fax: +81 75 761 9780.
E-mail address: ryosuket@kuhp.kyoto-u.ac.jp.

0014-4886/$ – see front matter
doi:10.1016/j.expneurol.2009.03.001

than those of control mice, suggesting that edaravone may improve the motor function of the ALS mice without apparent lifespan expanding effects (Ito et al., 2008). This uncoupling in the mechanisms underlying motor function and lifespan further implies that pathways causing motor function decline are not necessarily the ones causing eventual death, usually by respiratory muscle failure. That said, it would be possible to identify drugs that can improve the quality of life in ALS patients without affecting lifespan, which seems to be an easier goal compared with identifying lifespan-extending drugs for ALS. Moreover, it was clinically important that edaravone was effective even when administered after the disease onset. On the other hand, it would be intriguing to administer edaravone to ALS mice at their presymptomatic stage to understand how the point at which edaravone is used during the course of disease affects its outcome.

It is noted that high-dose edaravone treatment leads to a decrease of mutant SOD1 accumulation in the spinal cord. Since administration of edaravone resulted in a marked decrease of 3-nitrotyrosine/tyrosine ratio, a marker of oxidative stress, suppression of oxidative stress is likely to be upstream of the inhibition of aggregate formation (Kabashi and Durham, 2006; Valentine and Hart, 2003). It has long been debated how oxidative stress is induced by SOD1 mutations (Barber et al., 2006). Reduced enzymatic activity of SOD1 and generation of peroxynitrite due to aberrant copper chemistry have been proposed as plausible mechanism explaining "gain of toxic function" of mutant SOD1 (Beckman et al., 1993; Deng et al., 1993; Robberecht et al., 1994). However, the fact that a subgroup of SOD1 mutants retains full enzymatic activity and that H46R and H48Q mutants which completely lose binding sites for copper still cause ALS suggests that mechanisms unrelated to SOD1 activity may also be involved (Borchelt et al., 1994; Valentine et al., 2005; Wang et al., 2003). It has been shown that mutant SOD1 overexpression in a neuronal cell line leads to transcriptional repression of antioxidant proteins by reducing the level of transcriptional factor NRF2 (Kirby et al., 2005). It would be intriguing to investigate whether edaravone affects the level of NRF2 when administered to ALS mice.

Another interesting unresolved question is which cells are the targets of edaravone. Recently, it has been shown that motor neuron death in mutant SOD1 ALS mouse models is non-cell autonomous (Boillee et al., 2006; Yamanaka et al., 2008). In other words, mutant SOD1-expressing astroglial or miroglial cells promote motor neuron death. In this context, edarovone may decrease the aggregates in non-neuronal glial cells, resulting in amelioration of neurodegeneration. These questions should be addressed in further analysis in the future.

A recent systematic review of randomized controlled trials of antioxidant therapies against ALS including vitamin E and acetylcysteine has shown that there is no substantial evidence to support their clinical use (Orrell et al., 2008). However, the evidence for the bene cial effects of edaravone on human ALS patients awaits the publication of the results of a phase III clinical trial of ALS, currently ongoing in Japan (http://www.als.net/research/studies/tdfAnimalStudyList.asp).

Acknowledgment

I thank Roberto Gavinio for kindly editing this manuscript.

References

Barber, S.C., Mead, R.J., Shaw, P.J., 2006. Oxidative stress in ALS: a mechanism of neurodegeneration and a therapeutic target. Biochim. Biophys. Acta 1762, 1051–1067.

Beckman, J.S., Carson, M., Smith, C.D., Koppenol, W.H., 1993. ALS, SOD and peroxynitrite. Nature 364, 584.

Benatar, M., 2007. Lost in translation: treatment trials in the SOD1 mouse and in human ALS. Neurobiol. Dis. 26, 1–13.

Boillee, S., Yamanaka, K., Lobsiger, C.S., Copeland, N.G., Jenkins, N.A., Kassiotis, G., Kollias, G., Cleveland, D.W., 2006. Onset and progression in inherited ALS determined by motor neurons and microglia. Science 312, 1389–1392.

Borchelt, D.R., Lee, M.K., Slunt, H.S., Guarnieri, M., Xu, Z.S., Wong, P.C., Brown Jr., R.H., Price, D.L., Sisodia, S.S., Cleveland, D.W., 1994. Superoxide dismutase 1 with mutations linked to familial amyotrophic lateral sclerosis possesses signi cant activity. Proc. Natl. Acad. Sci. U. S. A. 91, 8292–8296.

Deng, H.X., Hentati, A., Tainer, J.A., Iqbal, Z., Cayabyab, A., Hung, W.Y., Getzoff, E.D., Hu, P., Herzfeldt, B., Roos, R.P. et al., 1993. Amyotrophic lateral sclerosis and structural defects in Cu,Zn superoxide dismutase. Science 261, 1047–1051.

Gurney, M.E., Pu, H., Chiu, A.Y., Dal Canto, M.C., Polchow, C.Y., Alexander, D.D., Caliendo, J., Hentati, A., Kwon, Y.W., Deng, H.X., et al., 1994. Motor neuron degeneration in mice that express a human Cu,Zn superoxide dismutase mutation. Science 264, 1772–1775.

Ito, H., Wate, R., Zhang, J., Ohnishi, S., Kaneko, S., Ito, H., Nakano, S., Kusaka, H., 2008. Treatment with edaravone, initiated at symptom onset, slows motor decline and decreases SOD1 deposition in ALS mice. Exp. Neurol. 213, 448–455.

Kabashi, E., Durham, H.D., 2006. Failure of protein quality control in amyotrophic lateral sclerosis. Biochim. Biophys. Acta 1762, 1038–1050.

Kirby, J., Halligan, E., Baptista, M.J., Allen, S., Heath, P.R., Holden, H., Barber, S.C., Loynes, C.A., Wood-Allum, C.A., Lunec, J., Shaw, P.J., 2005. Mutant SOD1 alters the motor neuronal transcriptome: implications for familial ALS. Brain 128, 1686–1706.

Mitchell, J.D., Borasio, G.D., 2007. Amyotrophic lateral sclerosis. Lancet 369, 2031–2041.

Neumann, M., Kwong, L.K., Sampathu, D.M., Trojanowski, J.Q., Lee, V.M., 2007. TDP-43 proteinopathy in frontotemporal lobar degeneration and amyotrophic lateral sclerosis: protein misfolding diseases without amyloidosis. Arch. Neurol. 64, 1388–1394.

Orrell, R.W., Lane, R.J., Ross, M., 2008. A systematic review of antioxidant treatment for amyotrophic lateral sclerosis/motor neuron disease. Amyotroph. Lateral Scler. 9, 195–211.

Robberecht, W., Sapp, P., Viaene, M.K., Rosen, D., McKenna-Yasek, D., Haines, J., Horvitz, R., Theys, P., Brown Jr., R., 1994. Cu/Zn superoxide dismutase activity in familial and sporadic amyotrophic lateral sclerosis. J. Neurochem. 62, 384–387.

Rosen, D.R., Siddique, T., Patterson, D., Figlewicz, D.A., Sapp, P., Hentati, A., Donaldson, D., Goto, J., O'Regan, J.P., Deng, H.X., et al., 1993. Mutations in Cu/Zn superoxide dismutase gene are associated with familial amyotrophic lateral sclerosis. Nature 362, 59–62.

Valentine, J.S., Hart, P.J., 2003. Misfolded CuZnSOD and amyotrophic lateral sclerosis. Proc. Natl. Acad. Sci. U. S. A. 100, 3617–3622.

Valentine, J.S., Doucette, P.A., Zittin Potter, S., 2005. Copper-zinc superoxide dismutase and amyotrophic lateral sclerosis. Annu. Rev. Biochem. 74, 563–593.

Wang, J., Slunt, H., Gonzales, V., Fromholt, D., Coon eld, M., Copeland, N.G., Jenkins, N.A., Borchelt, D.R., 2003. Copper-binding-site-null SOD1 causes ALS in transgenic mice: aggregates of non-native SOD1 delineate a common feature. Hum. Mol. Genet. 12, 2753–2764.

Yamanaka, K., Chun, S.J., Boillee, S., Fujimori-Tonou, N., Yamashita, H., Gutmann, D.H., Takahashi, R., Misawa, H., Cleveland, D.W., 2008. Astrocytes as determinants of disease progression in inherited amyotrophic lateral sclerosis. Nat. Neurosci. 11, 251–253.

Yoshida, H., Yanai, H., Namiki, Y., Fukatsu-Sasaki, K., Furutani, N., Tada, N., 2006. Neuroprotective effects of edaravone: a novel free radical scavenger in cerebrovascular injury. CNS Drug Rev. 12, 9–20.

Yoshino, H., Kimura, A., 2006. Investigation of the therapeutic effects of edaravone, a free radical scavenger, on amyotrophic lateral sclerosis (Phase II study). Amyotroph. Lateral. Scler. 7, 241–245.

Journal of Neuroscience Research 87:576–585 (2009)

Nicotinic Receptor Stimulation Protects Nigral Dopaminergic Neurons in Rotenone-induced Parkinson's Disease Models

Hiroki Takeuchi,[1] Takashi Yanagida,[2] Masatoshi Inden,[2] Kazuyuki Takata,[2] Yoshihisa Kitamura,[2] Kentaro Yamakawa,[3] Hideyuki Sawada,[3] Yasuhiko Izumi,[4] Noriyuki Yamamoto,[4] Takeshi Kihara,[4] Kengo Uemura,[1] Haruhisa Inoue,[1] Takashi Taniguchi,[2] Akinori Akaike,[4] Ryosuke Takahashi,[1] and Shun Shimohama[5]*

[1]Department of Neurology, Graduate School of Medicine, Kyoto University, Kyoto, Japan
[2]Department of Neurobiology, Kyoto Pharmaceutical University, Kyoto, Japan
[3]Clinical Research Center, National Hospital Organization Utano National Hospital, Kyoto, Japan
[4]Department of Pharmacology, Graduate School of Pharmaceutical Sciences, Kyoto University, Kyoto, Japan
[5]Department of Neurology, Sapporo Medical University, Sapporo, Japan

Parkinson's disease (PD) is the second most common neurodegenerative disease and is characterized by dopaminergic (DA) neuronal cell loss in the substantia nigra. Although the entire pathogenesis of PD is still unclear, both environmental and genetic factors contribute to neurodegeneration. Epidemiologic studies show that prevalence of PD is lower in smokers than in nonsmokers,. Nicotine, a releaser of dopamine from DA neurons, is one of the candidates of antiparkinson agents in tobacco. To assess the protective effect of nicotine against rotenone-induced DA neuronal cell toxicity, we examined the neuroprotective effects of nicotine in rotenone-induced PD models in vivo and in vitro. We observed that simultaneous subcutaneous administration of nicotine inhibited both motor deficits and DA neuronal cell loss in the substantia nigra of rotenone-treated mice. Next, we analyzed the molecular mechanisms of DA neuroprotective effect of nicotine against rotenone-induced toxicity with primary DA neuronal culture. We found that DA neuroprotective effects of nicotine were inhibited by dihydro-β-erythroidine (DHβE), α-bungarotoxin (αBuTx), and/or PI3K-Akt/PKB (protein serine/threonine kinase B) inhibitors, demonstrating that rotenone-toxicity on DA neurons are inhibited via activation of α4β2 or α7 nAChRs-PI3K-Akt/PKB pathway or pathways. These results suggest that the rotenone mouse model may be useful for assessing candidate antiparkinson agents, and that nAChR (nicotinic acetylcholine receptor) stimulation can protect DA neurons against degeneration. © 2008 Wiley-Liss, Inc.

Key words: Parkinson's disease; rotenone; nicotine; dopaminergic neuron; neuroprotection

Parkinson's disease (PD) is the second most common progressive neurodegenerative disorder. It is characterized by relatively selective degeneration of dopaminergic neurons in the substantia nigra and loss of dopamine in the striatum resulting in resting tremor, rigidity, bradykinesia and postural instability (Dunnett and Björklund, 1999; Shimohama et al., 2003). Although the pathogenesis of PD is still unclear, it is thought that both environmental and genetic factors cause neurodegeneration. Rural residency, pesticides and intrinsic toxic agents were reported as environmental risk factors for sporadic PD. Recent studies revealed several mutations in familial PD genes such as α-synuclein, parkin, PINK1, LRRK2 (leucine-rich repeat kinase 2), DJ-1, and UCH-L1 (ubiquitin C-terminal hydrolase-L1) (Schapira, 2006). Epidemiological studies suggest that the use of pesticides increases the risk of PD, possibly via reduced activity of complex I in the mitochondrial respiratory chain in the substantia nigra and result in the pathogenesis of PD (Parker et al., 1989; Mann et al., 1992; Mizuno et al., 1998). 6-hydroxydopamine (6-OHDA), a H_2O_2 pro-oxidant and 1-methyl-4-phenyl-1,2,3,6-tetrahydropyridine (MPTP), a mitochondrial complex I inhibitor, have been widely used to produce toxin models of sporadic PD. Chronic exposure to rotenone, a nature-derived pesticide, could be a more

*Correspondence to: Shun Shimohama, MD, PhD, Department of Neurology, Sapporo Medical University, S1W17, Chuo-ku, Sapporo, 060-8556, Japan. E-mail: shimoha@sapmed.ac.jp

Received 18 March 2008; Revised 28 May 2008; Accepted 13 July 2008

Published online 19 September 2008 in Wiley InterScience (www.interscience.wiley.com). DOI: 10.1002/jnr.21869

appropriate animal PD model because rotenone-treated animals show slowly progressive DA neuronal loss, and Lewy body–like particles, which are primarily aggregations of α-synuclein (Betarbet et al., 2000, Inden et al., 2007).

On the other hand, current drug therapy is limited to supplementing dopamine (DA) or enhancing dopaminergic effect. Some may have neuroprotective effects, but their effects remain controversial (Quik, 2004; Du et al., 2005; Iravani et al., 2006). It has also been reported that smokers have a lower risk for PD (De Reuck et al., 2005; Wirdefeldt et al., 2005), and nAChRs (nicotinic acetylcholine receptor) were decreased in the brains of PD patients (Fujita et al., 2006) and PD model animals (Quik et al., 2006). Nicotine may up-regulate DA release at striatum from nigral dopaminergic neurons (Morens et al., 1995), followed by stimulation of α4β2 nAChRs (Champtiaux et al., 2003). Furthermore, nicotine could protect mitochondria and had protective effect from oxidative stress (Cormier et al., 2003; Xie et al., 2005). In studies made in vivo, stimulation of nAChRs resulted in neuroprotection in cerebral ischemia and PD model animals (Shimohama et al., 1998; Kagitani et al., 2000; Parain et al., 2003). In vitro, we have demonstrated that nicotine protected rat cortical neurons against glutamate toxicity and lower motor neurons against β-amyloid toxicity respectively, and that nicotine was antiapoptotic (Akaike et al., 1994; Kihara et al., 1997, 2001; Nakamizo et al., 2005). Also nicotine protected rat nigral dopaminergic neurons against 1-methyl-4-phenylpyridinium (MPP^+) cytotoxicity by non-α7 nAChR stimulation (Jeyarasasingam et al., 2002). So nicotinic receptor stimulation may be a good target for DA neuroprotective therapy toward PD. However, the further protective mechanisms for dopaminergic neurons have not been elucidated.

In this study, we investigated the neuroprotective effect of nicotine against nigral DA neuronal death induced by rotenone with a chronic rotenone-treated PD mouse model, and analyzed molecular mechanisms of the protection in dissociated cultures of the fetal rat ventral mesencephalon.

MATERIALS AND METHODS

Materials

Rotenone, (−)-nicotine hydrogen bitartrate, mecamylamine (Mec), αBuTx, DHβE, and triciribine, an Akt/PKB inhibitor, were purchased from Sigma (St. Louis, MO). LY294002, a PI3K (phosphatidylinositol 3-kinase) inhibitor was from Calbiochem (Darmstadt, Germany). Carboxylmethyl cellulose (CMC) was obtained from Nacalai Tesque (Kyoto, Japan). Mouse monoclonal antibodies against microtubule-associated protein 2 (MAP2), tyrosine hydroxylase (TH) and β-actin were purchased from Sigma. Rabbit polyclonal antibody against TH was from Chemicon (Temecula, CA).

Mouse Model and Drug Administration

Eight-week-old male C57BL/6J mice (20–25 g) were purchased from Japan SLC Inc. (Hamamatsu, Japan). The animals were acclimated and maintained at 23°C under a 12-hr light/dark cycle (lights on 09.00–21.00 hr). Mice were housed in standard laboratory cages and had free access to food and water throughout the study period. All animal experiments were carried out in accordance with the National Institutes of Health (NIH) Guide for the Care and Use of Laboratory Animals, and the protocols were approved by the Committee for Animal Research at Kyoto University. Rotenone was administrated orally once daily by gavage with a catheter at a dose of 30 mg/kg for 28 days. Rotenone was suspended in 0.5% CMC and administrated orally once daily at a concentration of 12 mL/kg body weight. The 0.5% CMC was administrated orally as vehicle to control mice (Inden et al., 2007). For in vivo experiments, nicotine ((−)-nicotine hydrogen bitartrate dissolved in saline) at a dose of 0.21 or 0.42 mg/kg (free base) was daily injected subcutaneously at 30 min before each oral administration of rotenone. Saline was injected in parallel as the corresponding vehicle control. Each group contained 6–12 mice.

Behavior Analysis

The behavior of each mouse was assessed by the rotarod treadmill test. The rotarod treadmill (accelerating model 7750, Ugo Basile, Varese, Italy) consists of a plastic rod, 6 cm in diameter and 36 cm long, with a nonslippery surface 20 cm above the base (trip plate). This rod is divided into four equal sections by five discs (25 cm in diameter), which enables four mice to walk on the rod at the same time. In the present study, the accelerating rotor mode was used (10-grade speeds from 3.5 to 35 r.p.m. for 5 min). Time was recorded while mice were running on the rod (from when they were put on the rod to when they fell off).

Immunohistochemistry

Mice were perfused with 10 mM phosphate-buffered saline (PBS) and then 4% paraformaldehyde in 100 mM phosphate buffer (PB) under deep anesthesia with pentobarbital (100 mg/kg, intraperitoneal injection). After perfusion, the brain was quickly removed and postfixed for 2 days and then transferred to 15% sucrose solution in 100 mM PB at 4°C at least for 4 days. After cryoprotection, the brain was rapidly frozen by heat exchange from vaporized CO_2 gas (−70°C) and then sections (60 μm) were cut with a cryostat and collected in 100 mM PBS containing 0.3% Triton X-100 (PBS-T). After several washes, the sections were stored until use in a free-floating state at 4°C for immunohistochemical analysis.

Brain sections were incubated with primary rabbit polyclonal antibody to TH (1:10,000), for 3 days at 4°C, and next with biotinylated antibody to rabbit IgG (1:2000) for 2 hr at room temperature. Then the sections were incubated with avidin peroxidase (1:4000) with the ABC kit for 1 hr at room temperature. All sections were rinsed several times with PBS-T between incubations. Labeling was revealed by DAB (3-3′-diaminobenzidine tetrahydrochloride) with nickel ammonium, which yielded a dark blue color.

Stereological Analysis

The total number of dopaminergic neurons in both hemispheres of the substantia nigra pars compacta (SNC) was

estimated by means of a fractionator-sampling design (Gundersen et al., 1988; West et al., 1991) and a former report (Baquet et al., 2005). Briefly, staining with the anti-TH antibody delineated the mediodorsal boundary of the SNC in each 60 μm cryostat section. We used every third coronal section to perform an analysis starting with the first appearance of TH-positive neurons and extending to the most caudal parts of the SNC and including both hemispheres. Cell counts were made at automatically determined intervals by the StereoInvestigator, a morphometry and stereology software package (version 5.0; MicroBrightField, Colchester, VT), within an unbiased counting frame of known area (100 × 100 μm^2) superimposed on the image. Sections were viewed under 40× magnification on an Olympus (Tokyo, Japan) BA51 photomicroscope, the StereoInvestigator, thereby creating a systematic random sample of the area, randomly positioned the counting frame within the SNC. We defined 16 μm as the z-dimension of the counting brick with a 2-μm guard on each side. Stained cells were counted within the outlines defined by TH expression, and total estimates were obtained.

Immunoblotting

After repeated rotenone administration for 28 days, the striatum (mixture of both right and left tissues) in treated mice were rapidly removed and homogenized with eight volumes of 50 mM Tris-buffered saline (pH 7.4) containing protease inhibitor cocktail (Roche Diagnostics, Mannheim, Germany). After centrifugation at 50,000*g* for 30 min, the supernatant was used as cytosolic fraction. Aliquots of cytosolic fractions containing 10 μg of protein were subjected to sodium dodecyl sulfate-polyacrylamide gel electrophoresis (SDS-PAGE) and then immunoblotted with mouse monoclonal antibody against TH (1:5000) and reblotted with anti-β-actin antibody (1:10,000). For semiquantitative analysis, bands of TH on radiographic films were scanned with a CCD color scanner (ARCUS II, AGFA, Leverkusen, Germany). Densitometric analysis was performed by the public domain program NIH Image 1.56 (by Wayne Rasband at the U.S. National Institutes of Health).

Primary Neuronal Cultures of the Ventral Mesencephalon

Cultures of rat mesencephalic cells were established according to methods described previously (Sawada et al., 2004). Briefly, the ventral two-thirds of the mesencephalon were dissected from rat embryos on the 16th day of gestation. The dissected regions included dopaminergic neurons from the substantia nigra and the ventral tegmental area but not noradrenergic neurons from the locus ceruleus. Neurons were dissociated mechanically and plated out onto 0.1% polyethylenimine-coated plastic coverslips at a density of 1.3 × 10^5 cells/cm^2. The culture medium consisted of Eagle's minimum essential medium containing 10% fetal calf serum for the first 1–4 days in culture and horse serum from the 5th day onward. Cultures were maintained at 37°C in a humidified atmosphere of 5% CO_2. Only mature cultures (8 days in vitro) were used for experiments. The animals were treated in accordance with guidelines published in the NIH Guide for the Care and Use of Laboratory Animals.

Treatment of Cultures

All experiments were carried out in Eagle's minimum essential medium with 10% horse serum at 37°C. First of all, cultured neurons were exposed to rotenone for 48 hr, except for pretreatment of LY294002 for 10 min to cause PI3K inhibition. After that, to show the time course, cultured neurons were administrated rotenone and/or nicotine for 12, 24, and 48 hr. Nicotine and nAChR antagonists (Mec, αBuTx, DHβE) were added to the medium simultaneously with rotenone. The concentration of each antagonist was the maximal dosage that did not show cytotoxicity or interference among nAChRs. Ki values of αBuTx were 2.16 (1.56–3.01) nM for α7 nAChR and >10,000 nM for α4β2nAChR, and those of DHβE were 7700 (4510–13,100) nM for α7 nAChR and 24.6 (16.9–35.8) nM for α4β2 nAChR (Grinevich et al., 2005). To confirm PI3K inhibition, LY294002 was administrated 10 min before the additional treatment of rotenone and nicotine. Triciribine was used simultaneously with rotenone and nicotine to inhibit Akt/PKB.

Immunocytochemistry and Evaluation of Neurotoxicity in Neuronal Cultures

Immunostaining was used to evaluate the number of dopaminergic neurons. Cultured cells were incubated with polyclonal rabbit anti-TH antibody (1:400) overnight at 4°C, then with biotinylated secondary antibody (1:200), and conjugated to avidin peroxidase (1:200) by the ABC kit (Vector Laboratories, Burlingame, CA) at room temperature for 1 hr. After that, they were labeled with a DAB staining kit (Nacalai, Kyoto, Japan). Neurotoxicity in each experiment was defined as a reduction in the survival rate, which was expressed as percentage survival relative to the survival observed in control cultures. For primary cultures, at least 200 dopaminergic neurons were counted in 30 randomly selected fields at 100× (total magnification) in control cultures to determine the total number of neurons. The total number of neurons was assessed by the method, described above, but using the anti-MAP2 antibody.

RNA Preparation From Rat Mesencephalic Cells

Total cell RNA was extracted with the Isogen RNA Isolation Kit (Nippon Gene, Japan) as originally described elsewhere (Chomczynski and Sacchi, 1987). The concentration of the isolated total RNA was determined spectrophotometrically at 260 nm. The first strand cDNA was synthesized with a reverse transcriptase–polymerase chain reaction (RT-PCR) kit purchased from GE Healthcare Bioscience (Giles, UK). Briefly, reverse transcription (RT) was carried out in a 15-μL reaction mixture containing 5 μg total RNA, 5 μL Bulk first-strand reaction mix, 1 μL DTT solution, and 1 μL $pd(N)_6$ primer, by incubation at 42°C for 20 min followed by denaturation at 99°C for 5 min and then quick-chilled on ice. The second strand cDNA synthesis/PCR amplification was performed in a mixture of 2 μL RT product, 2.5 μL 10× PCR buffer, 200 nM dNTP, 1.5 mM $MgCl_2$, 0.05 U/μL Ex

TABLE 1. Paired Primers Used for RT-PCR Detection of nAChR Subunits*

Subunit	Primer	Nucleotide sequence	Size (bp)	Tm (°C)
α4	Forward	CTGGGTGCGTAGAGTCTTCC	239	62
	Reverse	TAGGCTGGGTCTCGACTGCT		
α7	Forward	TTTCTGCGCATGAAGAGGCCCGGAGAT	295	60
	Reverse	ACCTCCTCCAGGATCTT		
β2	Forward	AAGGTGGTCTTCCTGGAGAAGC	287	60
	Reverse	GCGTACGCCATCCACTGCT		
GAPDH	Forward	CGTCTTCACCACCATGGAGA	300	60
	Reverse	CGGCCATCACGCCACAGCTT		

*Tm, annealing temperature; Forward, sense primer; Reverse, antisense primer. GAPDH (glyceraldehyde-3-phosphate dehydrogenase) was used as the internal control for RNA detection.

Taq DNA polymerase, and 500 nM sense and antisense primers (Table I). The amplification protocol was as follows: initial denaturation at 94°C for 5 min; 30 cycles at 94°C for 30 sec, annealing at the respective temperature (Table I) for 30 sec, and 72°C for 1.5 min; a final extension at 72°C for 7 min with a GeneAmp 9700 thermal cycler (Perkin Elmer, Applied Biosystem, Forster City, CA). PCR products were electrophoresed on 2% agarose gels and stained with ethidium bromide (0.5 mg/mL). Then, the PCR products were visualized with an ultraviolet transilluminator coupled to a CCD camera.

Statistical Evaluation

Data was expressed as the ratio of surviving dopaminergic neurons relative to the number of neurons in vehicle-treated or in control group. Also, the density of TH by immunoblotting was assessed in the same manner. They are represented as the mean ± SEM. Statistical significance was determined by analysis of variance (ANOVA) followed by Bonferroni's multiple comparison test.

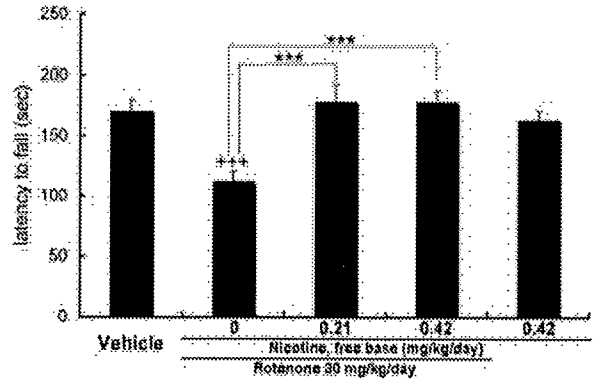

Fig. 1. Behavior analysis by rotarod treadmill test of chronically rotenone-treated mice. Nicotine administration improved impaired behavior induced by rotenone. One-way ANOVA was used for statistical analysis, followed by Bonferroni's multiple comparison test. Each value is the mean ± SEM, $n = 8$–12, $^{***}P < 0.001$, $^{+++}P < 0.001$ vs. vehicle.

RESULTS

Nicotine Treatment Improved Behavior Impaired by Rotenone

In our in vivo studies, we first checked the motor behavior of rotenone-treated model mice because it was important that the animals showed a close PD phenotype. The simultaneous daily administration of oral rotenone and subcutaneous nicotine prevented the motor impairment elicited by rotenone (Fig. 1). Nicotine alone showed no significant difference compared with the vehicle group. This animal model could be useful for assessing the bradykinesia/akinesia, one of the symptoms of PD.

Nicotine Treatment Improved Histological Findings in the Substantia Nigra

In the substantia nigra, oral treatment of rotenone decreased the number of dopaminergic neurons. On the other hand, the simultaneous daily administration of oral rotenone and subcutaneous nicotine prevented the decrease (Fig. 2A). Stereological assessment of the number of TH-positive cells in the bilateral SNC confirmed the histological findings with the statistical significance (Fig. 2B). That is, simultaneous administration of nicotine significantly protected dopaminergic cells in the midbrain of rotenone-treated mice from rotenone-induced neurotoxicity.

Nicotine Attenuated Rotenone-induced Axonal/Nerve Terminal Damage in the Striatum

The striatum was immunostained with the same antibody as the substantia nigra. About histological findings, the density of TH-positive neurons in the striatum of rotenone-treated mice seemed to be diminished compared with the vehicle group. Rotenone and nicotine treatment seemed to prevent the density from being decreased (Fig. 3A). Densitometric analysis of immunoblotting performed using the striatal lysate of each group showed that nicotine treatment remarkably improved the expression of TH from rotenone toxicity (Fig. 3B). In other words, these results confirmed that nicotine protected nigrostriatal dopaminergic neurons from the cell death by rotenone toxicity. α-Synuclein-positive aggregations were detected in the cell bodies of dopaminergic neurons of rotenone-treated mice, but the number was

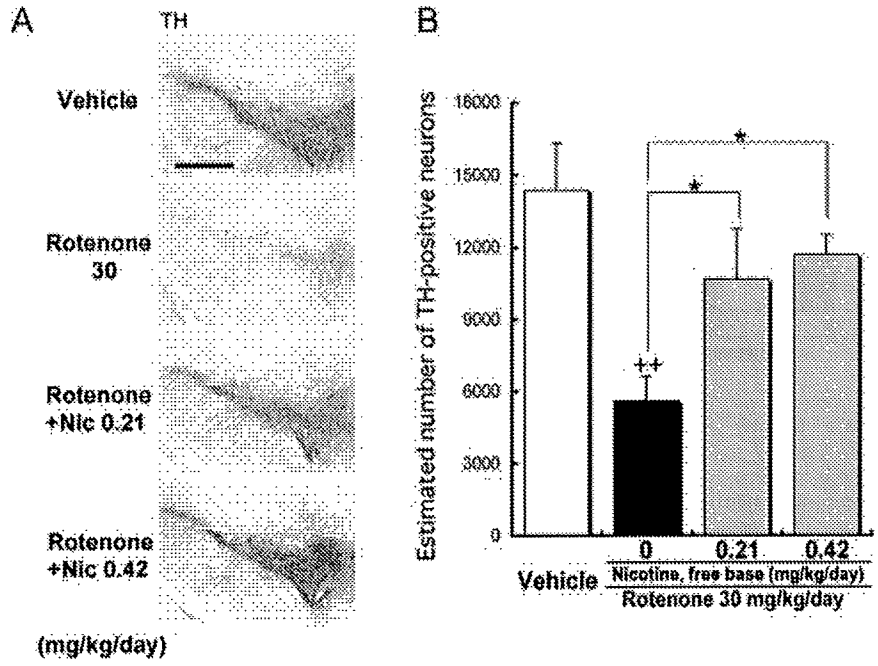

Fig. 2. Immunohistological analysis of nigral dopamine neurons. Nicotine improved the viability of dopaminergic cells against rotenone toxicity. Nic, Nicotine. **A:** Representative findings of each group. Scale bar = 500 μm. **B:** Stereological analysis of the number of the TH-positive neurons in the substantia nigra. One-way ANOVA was used for statistical analysis, followed by Bonferroni's multiple comparison test. Each value is the mean ± SEM, $n = 4$, $^{*}P < 0.05$, $^{++}P < 0.01$ vs. vehicle.

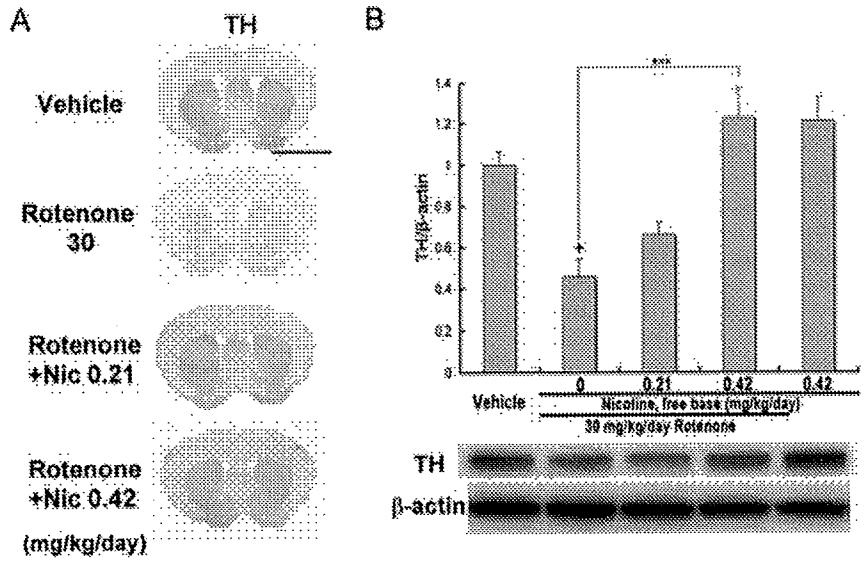

Fig. 3. Immunological analysis of striatal dopamine neurons. Nicotine improved the viability of dopaminergic cells against rotenone toxicity. **A:** Representative immunohistological findings of each group. Nic, Nicotine. Scale bar = 4 mm. **B:** Densitometric analysis of TH in striatal lysate. TH density was expressed as TH/β-actin ratio and relative density standardized by the results of vehicle group. One-way ANOVA was used for statistical analysis, followed by Bonferroni's multiple comparison test. Each value is the mean ± SEM, $n = 4$, $^{***}P < 0.001$, $^{+}P < 0.05$ vs. vehicle.

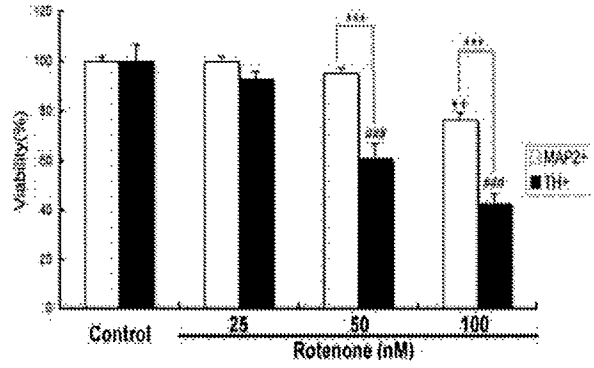

Fig. 4. Statistical analysis of rotenone-induced neuronal cell death in cultures of rat mesencephalic cells (day 8), standardized by the number of sham operations. It was suggested that dopaminergic neuron was more vulnerable against rotenone toxicity than other types of neurons. MAP2, microtubule-associated protein 2, a marker of central nervous system neurons; TH, tyrosine hydroxylase, a marker of dopaminergic neurons. Two-way factorial ANOVA was used for statistical analysis, followed by Bonferroni's multiple comparison test. Each value is the mean ± SEM, $n = 8$, $^{***}P < 0.001$, $^{++}P < 0.01$ vs. control (MAP2 positive), $^{###}P < 0.001$ vs. control (TH positive).

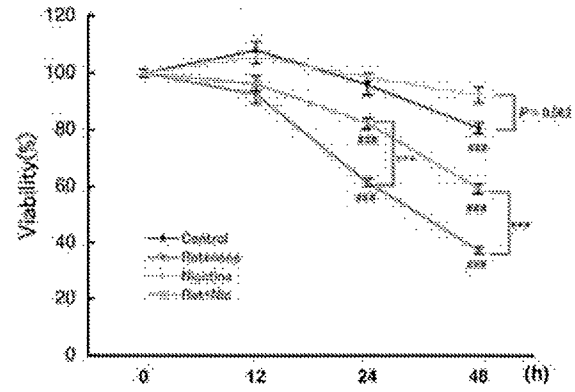

Fig. 5. Time course analysis of rotenone toxicity and nicotinic neuroprotection for TH-positive neurons, standardized by the number of control 0 hr. Both effects were shown after 24 hr since compounds were administrated. Rotenone, rotenone 100 nM; Nicotine, nicotine 100 μM; Rot+Nic, simultaneous administration of rotenone 100 nM and nicotine 100 μM. Two-way factorial ANOVA was used for statistical analysis, followed by Bonferroni's multiple comparison test. Each value is the mean ± SEM, $n = 8$, $^{###}P < 0.001$ vs. control 0 hr, $^{+++}P < 0.001$ vs. rotenone 24 hr, $^{***}P < 0.001$ vs. rotenone 48 hr.

too small to perform statistical assessment (data not shown).

Neuroprotective Effect of Nicotine Against Rotenone-induced Neurotoxicity in Cultures of Mesencephalic Neurons

Forty-eight-hour exposure to rotenone caused dose-dependent neurotoxicity, more remarkable in TH-positive neurons than in MAP2-positive cells, which represented the total neuronal cells (Fig. 4). This result showed that dopaminergic neurons were more vulnerable to rotenone-induced neurotoxicity. Time course experiment revealed that both rotenone toxicity and nicotinic neuroprotection were shown remarkably after 24 hr (Fig. 5). Immunostaining of TH showed that the viability of TH-positive cells was decreased by rotenone treatment and improved by addition of nicotine. Treatment with nicotine alone did not remarkably change the viability of TH-positive cells statistically (Fig. 5, Fig. 6A–D). Simultaneous administration of nicotine resulted in a dose-dependent increase of the viability of TH-positive cells (Fig. 6E). So nicotine treatment protected dopaminergic neurons against rotenone-induced neuronal death in a dose-dependent manner. This neuroprotective effect was inhibited by 100 μM Mec, a broad-spectrum nAChR antagonist (Fig. 7A), 100 nM αBuTx, an α7 nAChR antagonist (Fig. 7B), and 1 μM DHβE, an α4β2 antagonist (Fig. 7C). Treatment with the same concentrations of these antagonists or nicotine alone did not affect neurotoxicity. Nicotine-induced neuroprotection was therefore shown to occur via nAChRs, at least through α7 and α4β2 receptors. Also, RT-PCR (Fig. 7D) showed that mRNA of nAChRs subunits was expressed in rat mesencephalic cells. These results are relevant to the previous report that α7 and α4β2 nAChRs had biological activity in dopaminergic neurons in the midbrain (Champtiaux et al., 2003).

Nicotine-induced PI3K-Akt/PKB Pathway-activated Survival Activity of Dopaminergic Neurons

LY294002, a PI3K inhibitor inhibited nicotinic neuroprotection (Fig. 8A). Also triciribine, an Akt/PKB inhibitor, had the same effect (Fig. 8B). It is therefore likely that nicotine could activate the PI3K-Akt/PKB pathway or pathways and increased survival of mesencephalic dopaminergic cells against rotenone-induced cell death.

DISCUSSION

Rotenone works as a mitochondrial complex I inhibitor. Acute lethal doses of rotenone eliminate the mitochondrial respiratory system of the cell, resulting in an anoxic status that immediately causes cell death. At sublethal doses, it causes partial inhibition of mitochondrial complex I, and in this situation mitochondrial dysfunction leads to increased oxidative stress, decreased ATP production, increased aggregation of unfolded proteins, and then activated apoptotic pathway or pathways that result in cell death (Betarbet et al., 2000), resembling DA neurodegeneration in PD. Our data in vivo suggest that nicotine attenuated dopaminergic neuronal death of orally rotenone-treated PD model mice. It was relevant to the reports about the forebrain of rat models

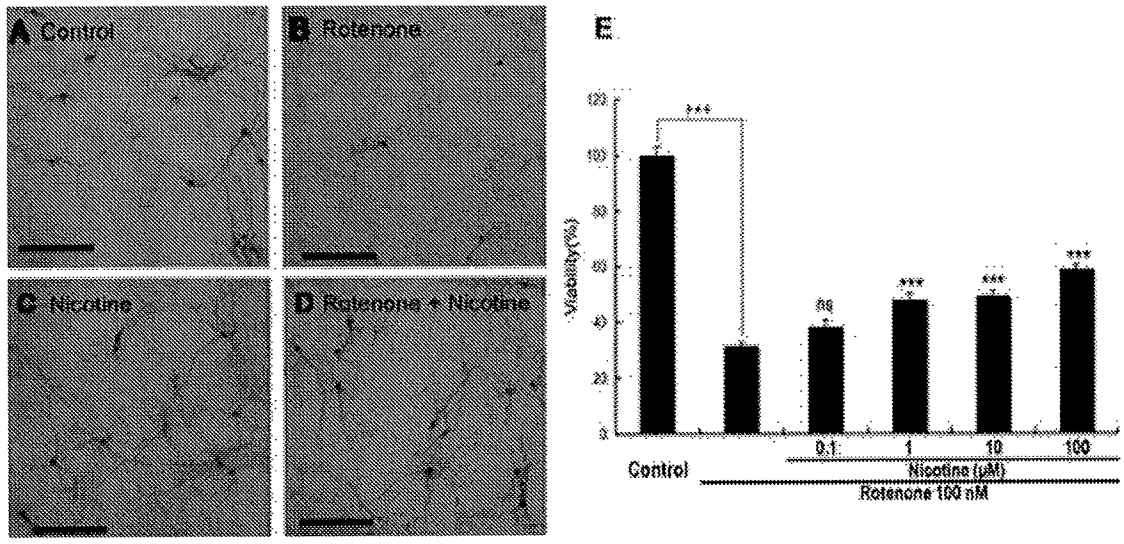

Fig. 6. Effect of nicotine on TH-positive neurons. Nicotine showed dose-dependent neuroprotection for dopaminergic neurons. A–D: Representative findings of each group of dopaminergic neurons. **A:** Control. **B:** Rotenone 100 nM. **C:** Nicotine 100 μM. **D:** Rotenone and nicotine added simultaneously for 48 hr. Scale bar = 200 μm. **E:** Statistical analysis of the viability of TH-positive cells, standardized by the number of control. Each value is the mean ± SEM, $n = 8$, $^{***}P < 0.001$ vs. rotenone 100 nM, $^{+++}P < 0.001$.

(Cormier et al., 2003), as well as about 6-OHDA models (Visanji et al., 2006). Our orally rotenone-treated mouse model showed motor deficits, dopaminergic cell death in the substantia nigra, nerve terminal/axonal loss in the striatum. These findings are relevant to some previous reports about rotenone PD models (Schmidt and Alam, 2006; Ravenstijn et al., 2008). However, some failed to make animal PD models by rotenone (Lapointe et al., 2004; Höglinger et al., 2006). Although the mechanism is unclear, these inconsistencies may arise from the differences in animal species or mode of compound delivery (Quik et al., 2007b). Our data suggest that nicotinic protection might be more remarkable in cell bodies than in axon or nerve terminals. That was relevant to the previous reports about paraquat-induced (Khwaja et al., 2007) or MPTP-induced (Parain et al., 2003) mouse models, both mitochondrial complex I inhibitors, and rotarod treadmill test was reported to be useful for evaluating motor deficits in MPTP-treated mouse models of parkinsonism (Rozas et al., 1998).

The present data showed nicotinic neuroprotection was via nAChRs, and RT-PCR suggested that both α7 and α4β2 nAChRs expressed on rat mesencephalic cells, whether they were on neurons or not. A previous report about the protective effect of nicotine against neurotoxicity suggested that a non-α7 receptor was involved (Jeyarasasingam et al., 2002). Our data showed that both α7 and α4β2 receptors had relationships with neuroprotection. We have previously shown that neuronal α7 nAChR stimulation appeared to activate the PI3K-Akt/PKB pathway or pathways, leading to induced expression of antiapoptotic B cell lymphoma protein–mediating neuronal survival in Aβ-potentiated glutamate-induced neurotoxicity (Kihara et al., 2001). On the other hand, neuronal α4β2 nAChR stimulation causes DA release (Champtiaux et al., 2003), and our data showed the neuroprotective effect also occurred via α4β2 nAChRs, so the mechanism of neuroprotection could vary for different receptor subclasses. In addition, we have also shown the protective effect of dopamine D2 receptor agonists in cortical neurons via the PI3K cascade (Kihara et al., 2002). Also other nAChR subclasses were reported to be protective (Visanji et al., 2006), and nAChR agonists were protective. Previously it was reported that α4β2 nAChR stimulation might improve behavior of PD models (O'Neill et al., 2002), and epibatidine protected bovine chromaffin cells against rotenone-induced toxicity (Egea et al., 2007). We could not examine the effect of α6β2 nAChR stimulation, but it was reported to be neuroprotective (Quik and McIntosh, 2006). Further studies should be needed to assess other nAChRs by using other nAChR agonists or nicotinic components.

Our primary cultures contained not only neuronal cells but also glial cells, so glial cells may also be partly responsible for nicotinic neuroprotection. Microglial cells have α7 nAChRs whose stimulation reduced the release of cytotoxic cytokines such as TNFα (Suzuki et al., 2006) and then decreased the activity of neuronal NF-κB (Liu et al., 2007). Chronically nicotine-treated rats might have NGF up-regulation in astrocytes of the

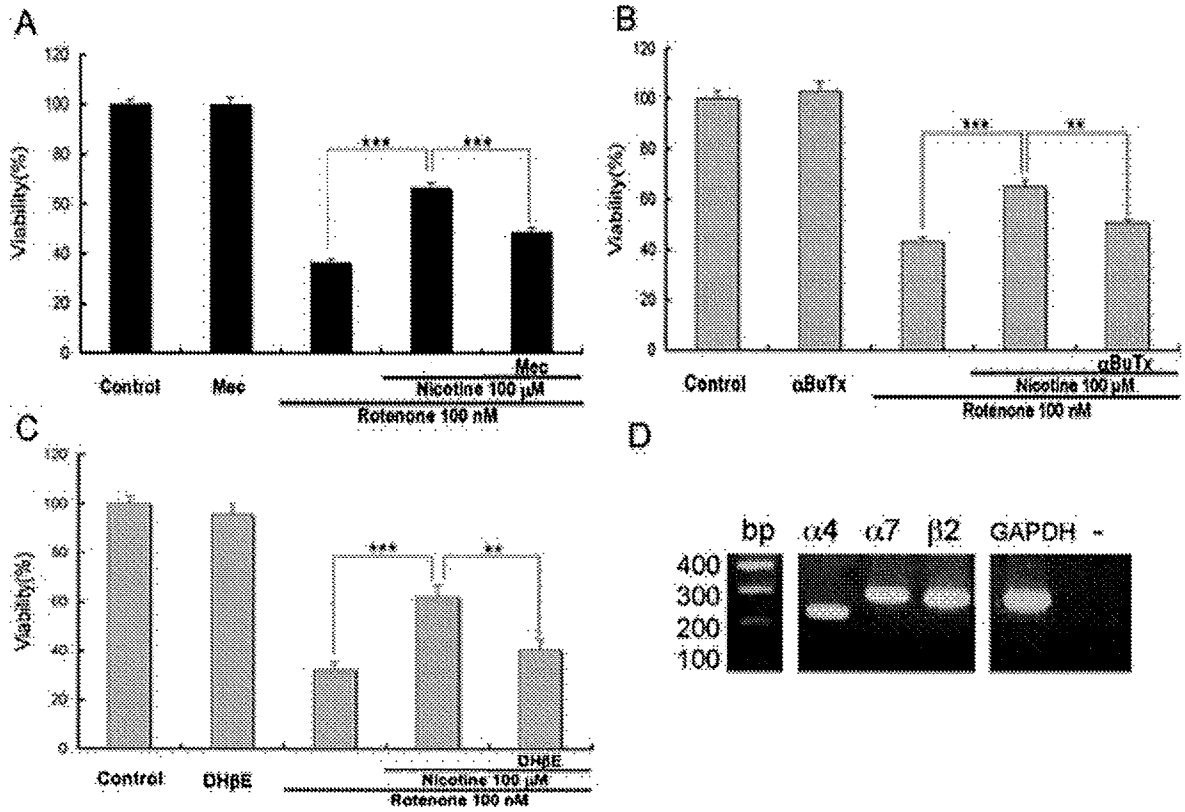

Fig. 7. A–C: Simultaneous administration of nicotinic acetylcholine receptor (nAChR) antagonists. Each antagonist blocked nicotinic neuroprotection, so it was suggested receptor-mediated. **A:** Mec, mecamylamine 100 μM, a broad-spectrum antagonist of nAChRs. **B:** αBuTx, α-bungarotoxin 100 nM, an α7 nAChR antagonist. **C:** DHβE, dihydro-β-erythroidine 1 μM, an α4β2 nAChR antagonist. Each value is the mean ± SEM, $n = 8$, $^{**}P < 0.01$, $^{***}P < 0.001$. **D:** Representative expression of mRNA for subunits of nAChRs in cultures of rat mesencephalic cells (day 8), RT-PCR products on an ethidium-bromide-stained gel. bp, number of base pairs; GAPDH, glyceraldehyde-3-phosphate dehydrogenase, which served as the internal control; −, negative control. Expression of mRNA for each α4,α7 and β2 subunit was remarkable. Paired primers used were indicated in Table I. The same results were obtained three times.

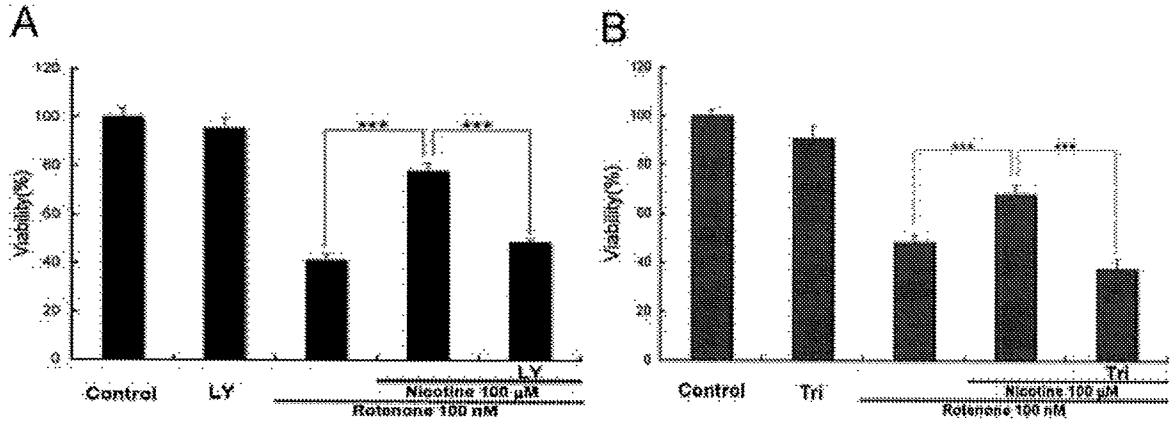

Fig. 8. Effects of the inhibitors of the PI3K-Akt/PKB pathway. Inhibition of either PI3K or Akt/PKB suppressed neuroprotective effect of nicotine. **A:** LY, LY294002 10 μM, an inhibitor of PI3K. **B:** Tri, triciribine 1 μM, an inhibitor of Akt/PKB. Each value is the mean ± SEM, $n = 8$, $^{***}P < 0.001$.

frontoparietal cortex (Martínez-Rodríguez et al., 2003). Nicotine decreased the number of activated microglial cells and TNFα and then protected dopaminergic neurons of MPTP-treated mice (Park et al., 2007). So glial cells may also play a role for the mechanism of the neuroprotection we have seen in the present study. We should also analyze glial neuroprotection by nicotine.

As mentioned above, other compounds that stimulate nAChRs show functional improvement in nonhuman primates (Quik et al., 2006, 2007a) and have neuroprotective effects are now on clinical trial, but the results were controversial. For example, SIB-1508Y, an α4β2 nAChR agonist, failed to improve symptoms of PD (Parkinson Study Group, 2006). Some cholinesterase inhibitors, for example, galantamine is an allosteric potentiating ligand (Santos et al., 2002) and stimulates cholinergic neurons in the nucleus basalis of Meynert, were reported to be effective for cognitive dysfunction of PD with dementia and Lewy body disease, a parkinsonism with hallucination and fluctuating dementia (Burn et al., 2006; Mentis et al., 2006, Miyasaki et al., 2006), but there may be deterioration of motor dysfunction due to simultaneous muscarinic acetylcholine receptor stimulation in the striatum. Thus, further analysis of glial neuroprotective effect by nicotine may be needed.

In conclusion, by stimulating nAChRs, the PI3K-Akt/PKB pathway or pathways could be activated to suppress dopaminergic cell death induced by rotenone. Additionally, chronic oral administration of rotenone induced motor deficits and nigrostriatal dopaminergic neurodegeneration in C57/BL6 mice, and nicotine attenuated both of them. These results suggest that derivatives of nicotine or agents that stimulate nAChRs may be useful for neuroprotective therapies targeting PD. In addition, rotenone-treated mice may be useful for understanding the mechanisms of dopaminergic cell death and may serve as a model of environmental factors involved in PD pathogenesis.

ACKNOWLEDGMENTS

This work was supported in part by the 21st Century Center of Excellence (COE) Program, the grants from Ministry of Education, Culture, Sports, Science and Technology of Japan, Japan Society for the Promotion of Science, Ministry of Health, Labour and Welfare of Japan, Smoking Research Foundation, and Philip Morris USA Inc. and Philip Morris International.

We thank to Megumi Asada-Utsugi, School of Health Sciences, Faculty of Medicine, Kyoto University, for contributing to the RT-PCR analysis.

REFERENCES

Akaike A, Tamura Y, Yokota T, Shimohama S, Kimura J. 1994. Nicotine-induced protection of cultured cortical neurons against N-methyl-D-aspartate receptor–mediated glutamate cytotoxicity. Brain Res 644:181–187.

Baquet Z, Bickford P, Jones K. 2005. Brain-derived neurotrophic factor is required for the establishment of the proper number of dopaminergic neurons in the substantia nigra pars compacta. J Neurosci 25:6251–6259.

Betarbet R, Sherer T, MacKenzie G, Garcia-Osuna M, Panov A, Greenamyre J. 2000. Chronic systemic pesticide exposure reproduces features of Parkinson's disease. Nat Neurosci 3:1301–1306.

Burn D, Emre M, McKeith I, De Deyn P, Aarsland D, Hsu C, Lane R. 2006. Effects of rivastigmine in patients with and without visual hallucinations in dementia associated with Parkinson's disease. Mov Disord 21:1899–1907.

Champtiaux N, Gotti C, Cordero-Erausquin M.David D, Przybylski C, Léna C, Clementi F, Moretti M, Rossi F, Le Novère N, McIntosh J, Gardier A, Changeux J. 2003. Subunit composition of functional nicotinic receptors in dopaminergic neurons investigated with knock-out mice. J Neurosci 23:7820–7829.

Chomczynski P, Sacchi N. 1987. Single-step method of RNA isolation by acid guanidinium thiocyanate-phenol-chloroform extraction. Anal Biochem 162:156–159.

Cormier A, Morin C, Zini R, Tillement J, Lagrue G. 2003. Nicotine protects rat brain mitochondria against experimental injuries. Neuropharmacology 44:642–652.

De Reuck J, De Weweire M, Van Maele G, Santens P. 2005. Comparison of age of onset and development of motor complications between smokers and non-smokers in Parkinson's disease. J Neurol Sci 231:35–39.

Du F, Li R, Huang Y, Li X, Le W. 2005. Dopamine D3 receptor-preferring agonists induce neurotrophic effects on mesencephalic dopamine neurons. Eur J Neurosci 22:2422–2430.

Dunnett S, Björklund A. 1999. Prospects for new restorative and neuroprotective treatments in Parkinson's disease. Nature 399:A32–A39.

Egea J, Rosa A, Cuadrado A, García A, López M. 2007. Nicotinic receptor activation by epibatidine induces heme oxygenase-1 and protects chromaffin cells against oxidative stress. J Neurochem 102:1842–1852.

Fujita M, Ichise M, Zoghbi S, Liow J, Ghose S, Vines D, Sangare J, Lu J, Cropley V, Iida H, Kim K, Cohen R, Bara-Jimenez W, Ravina B, Innis R. 2006. Widespread decrease of nicotinic acetylcholine receptors in Parkinson's disease. Ann Neurol 59:174–177.

Grinevich V, Letchworth S, Lindenberger K, Menager J, Mary V, Sadieva K, Buhlman L, Bohme G, Pradier L, Benavides J, Lukas R, Bencherif M. 2005. Heterologous expression of human α6β4β3α5 nicotinic acetylcholine receptors: binding properties consistent with their natural expression require quaternary subunit assembly including the α5 subunit. J Pharmacol Exp Ther 312:619–626.

Gundersen H, Bendtsen T, Korbo L, Marcussen N, Møller A, Nielsen K, Nyengaard J, Pakkenberg B, Sørensen F, Vesterby A. 1988. Some new, simple and efficient stereological methods and their use in pathological research and diagnosis. APMIS 96:379–394.

Höglinger G, Oertel W, Hirsch E. 2006. The rotenone model of parkinsonism—the five years inspection. J Neural Transm Suppl 70:269–272.

Inden M, Kitamura Y, Takeuchi H, Yanagida T, Takata K, Kobayashi Y, Taniguchi T, Yoshimoto K, Kaneko M, Okuma Y, Taira T, Ariga H, Shimohama S. 2007. Neurodegeneration of mouse nigrostriatal dopaminergic system induced by repeated oral administration of rotenone is prevented by 4-phenylbutyrate, a chemical chaperone. J Neurochem 101:1491–1504.

Iravani M, Haddon C, Cooper J, Jenner P, Schapira A. 2006. Pramipexole protects against MPTP toxicity in non-human primates. J Neurochem 96:1315–1321.

Jeyarasasingam G, Tompkins L, Quik M. 2002. Stimulation of non-α7 nicotinic receptors partially protects dopaminergic neurons from 1-methyl-4-phenylpyridinium-induced toxicity in culture. Neuroscience 109:275–285.

Kagitani F, Uchida S, Hotta H, Sato A. 2000. Effects of nicotine on blood flow and delayed neuronal death following intermittent transient ischemia in rat hippocampus. Jpn J Physiol 50:585–595.

Khwaja M, McCormack A, McIntosh J, Di Monte D, Quik M. 2007. Nicotine partially protects against paraquat-induced nigrostriatal damage in mice; link to alpha6beta2* nAChRs. J Neurochem 100:180–190.

Kihara T, Shimohama S, Sawada H, Kimura J, Kume T, Kochiyama H, Maeda T, Akaike A. 1997. Nicotinic receptor stimulation protects neurons against beta-amyloid toxicity. Ann Neurol 42:159–163.

Kihara T, Shimohama S, Sawada H, Honda K, Nakamizo T, Shibasaki H, Kume T, Akaike A. 2001. α7 nicotinic receptor transduces signals to phosphatidylinositol 3-kinase to block Abeta-amyloid-induced neurotoxicity. J Biol Chem 276:13541–13546.

Kihara T, Shimohama S, Sawada H, Honda K, Nakamizo T, Kanki R, Yamashita H, Akaike A. 2002. Protective effect of dopamine D2 agonists in cortical neurons via the phosphatidylinositol 3 kinase cascade. J Neurosci Res 70:274–282.

Lapointe N, St-Hilaire M, Martinoli M, Blanchet J, Gould P, Rouillard C, Cicchetti F. 2004. Rotenone induces non-specific central nervous system and systemic toxicity. FASEB J 18:717–719.

Liu Q, Zhang J, Zhu H, Qin C, Chen Q, Zhao B. 2007. Dissecting the signaling pathway of nicotine-mediated neuroprotection in a mouse Alzheimer disease model. FASEB J 21:61–73.

Martínez-Rodríguez R, Toledano A, Alvarez M, Turégano L, Colman O, Rosés P, Gómez de Segura I, De Miguel E. 2003. Chronic nicotine administration increases NGF-like immunoreactivity in frontoparietal cerebral cortex. J Neurosci Res 73:708–716.

Mann V, Cooper J, Krige D, Daniel S, Schapira A, Marsden C. 1992. Brain, skeletal muscle and platelet homogenate mitochondrial function in Parkinson's disease. Brain 115(Pt 2):333–342.

Mentis M, Delalot D, Naqvi H, Gordon M, Gudesblatt M, Edwards C, Donatelli L, Dhawan V, Eidelberg D. 2006. Anticholinesterase effect on motor kinematic measures and brain activation in Parkinson's disease. Mov Disord 21:549–555.

Miyasaki J, Shannon K, Voon V, Ravina B, Kleiner-Fisman G, Anderson K, Shulman L, Gronseth G, Weiner W;Quality Standards Subcommittee of the American Academy of Neurology. 2006. Practice Parameter: evaluation and treatment of depression, psychosis, and dementia in Parkinson disease (an evidence-based review): report of the Quality Standards Subcommittee of the American Academy of Neurology. Neurology 66:996–1002.

Mizuno Y, Yoshino H, Ikebe S, Hattori N, Kobayashi T, Shimoda-Matsubayashi S, Matsumine H, Kondo T. 1998. Mitochondrial dysfunction in Parkinson's disease. Ann Neurol 44(3 Suppl 1):S99–S109.

Morens D, Grandinetti A, Reed D, White L, Ross G. 1995. Cigarette smoking and protection from Parkinson's disease: false association or etiologic clue? Neurology 45:1041–1051.

Nakamizo T, Kawamata J, Yamashita H, Kanki R, Kihara T, Sawada H, Akaike A, Shimohama S. 2005. Stimulation of nicotinic acetylcholine receptors protects motor neurons. Biochem Biophys Res Commun 330:1285–1289.

O'Neill M, Murray T, Lakies V, Visanji N, Duty S. 2002. The role of neuronal nicotinic acetylcholine receptors in acute and chronic neurodegeneration. Curr Drug Targets CNS Neurol Disord 1:399–411.

Parain K, Hapdey C, Rousselet E, Marchand V, Dumery B, Hirsch E. 2003. Cigarette smoke and nicotine protect dopaminergic neurons against the 1-methyl-4-phenyl-1,2,3,6-tetrahydropyridine Parkinsonian toxin. Brain Res 984:224–232.

Park H, Lee P, Ahn Y, Choi Y, Lee G, Lee D, Chung E, Jin B. 2007. Neuroprotective effect of nicotine on dopaminergic neurons by anti-inflammatory action. Eur J Neurosci 26:79–89.

Parker W Jr, Boyson S, Parks J. 1989. Abnormalities of the electron transport chain in idiopathic Parkinson's disease. Ann Neurol 26:719–723.

Parkinson Study Group. 2006. Randomized placebo-controlled study of the nicotinic agonist SIB-1508Y in Parkinson disease. Neurology 66:408–410.

Quik M. 2004. Smoking, nicotine and Parkinson's disease. Trends Neurosci 27:561–568.

Quik M, McIntosh J. 2006. Striatal alpha6* nicotinic acetylcholine receptors: potential targets for Parkinson's disease therapy. J Pharmacol Exp Ther 316:481–489.

Quik M, Chen L, Parameswaran N, Xie X, Langston J, McCallum S. 2006. Chronic oral nicotine normalizes dopaminergic function and synaptic plasticity in 1-methyl-4-phenyl-1,2,3,6- tetrahydropyridine-lesioned primates. J Neurosci 26:4681–4689.

Quik M, Cox H, Parameswaran N, O'Leary K, Langston J, Di Monte D. 2007a. Nicotine reduces levodopa-induced dyskinesias in lesioned monkeys. Ann Neurol 62:588–596.

Quik M, O'Neill M, Perez X. 2007b. Nicotine neuroprotection against nigrostriatal damage: importance of the animal model. Trends Pharmacol Sci 28:229–235.

Ravenstijn P, Merlini M, Hameetman M, Murray T, Ward M, Lewis H, Ball G, Mottart C, de Ville de Goyet C, Lemarchand T, van Belle K, O'Neill M, Danhof M, de Lange E. 2008. The exploration of rotenone as a toxin for inducing Parkinson's disease in rats, for application in BBB transport and PK-PD experiments. J Pharmacol Toxicol Methods 57:114–130.

Rozas G, Liste I, Guerra M, Labandeira-Garcia J. 1998. Sprouting of the serotonergic afferents into striatum after selective lesion of the dopaminergic system by MPTP in adult mice. Neurosci Lett 245:151–154.

Santos M, Alkondon M, Pereira E, Aracava Y, Eisenberg H, Maelicke A, Albuquerque E. 2002. The nicotinic allosteric potentiating ligand galantamine facilitates synaptic transmission in the mammalian central nervous system. Mol Pharmacol 61:1222–1234.

Sawada H, Kohno R, Kihara T, Izumi Y, Sakka N, Ibi M, Nakanishi M, Nakamizo T, Yamakawa K, Shibasaki H, Yamamoto N, Akaike A, Inden M, Kitamura Y, Taniguchi T, Shimohama S. 2004. Proteasome mediates dopaminergic neuronal degeneration, and its inhibition causes alpha-synuclein inclusions. J Biol Chem 279:10710–10719.

Schapira A. 2006. Etiology of Parkinson's disease. Neurology 66(10 Suppl 4):S10–S23.

Schmidt W, Alam M. 2006. Controversies on new animal models of Parkinson's disease pro and con: the rotenone model of Parkinson's disease (PD). J Neural Transm Suppl 70:273–276.

Shimohama S, Greenwald D, Shafron D, Akaike A, Maeda T, Kaneko S, Kimura J, Simpkins C, Day A, Meyer E. 1998. Nicotinic α7 receptors protect against glutamate neurotoxicity and neuronal ischemic damage. Brain Res 779:359–363.

Shimohama S, Sawada H, Kitamura Y, Taniguchi T. 2003. Disease model: Parkinson's disease. Trends Mol Med 9:360–365.

Suzuki T, Hide I, Matsubara A, Hama C, Harada K, Miyano K, Andrä M, Matsubayashi H, Sakai N, Kohsaka S, Inoue K, Nakata Y. 2006. Microglial α7 nicotinic acetylcholine receptors drive a phospholipase C/IP3 pathway and modulate the cell activation toward a neuroprotective role. J Neurosci Res 83:1461–1470.

Visanji N, O'Neill M, Duty S. 2006. Nicotine, but neither the alpha4-beta2 ligand RJR2403 nor an alpha7 nAChR subtype selective agonist, protects against a partial 6-hydroxydopamine lesion of the rat median forebrain bundle. Neuropharmacology 51:506–516.

West M, Slomianka L, Gundersen J. 1991. Unbiased stereological estimation of the total number of neurons in the subdivisions of the rat hippocampus using the optical fractionator. Anat Rec 231:482–497.

Wirdefeldt K, Gatz M, Pawitan Y, Pedersen N. 2005. Risk and protective factors for Parkinson's disease: a study in Swedish twins. Ann Neurol 57:27–33.

Xie Y, Bezard E, Zhao B. 2005. Investigating the receptor-independent neuroprotective mechanisms of nicotine in mitochondria. J Biol Chem 280:32405–32412.

Journal of Neurochemistry JNC

JOURNAL OF NEUROCHEMISTRY | 2009 | 108 | 350–360 doi: 10.1111/j.1471-4159.2008.05760.x

N-cadherin-based adhesion enhances Aβ release and decreases $A\beta_{42/40}$ ratio

Kengo Uemura,* Christina M. Lill,† Mary Banks,† Megumi Asada,‡ Nobuhisa Aoyagi,* Koichi Ando,* Masakazu Kubota,‡ Takeshi Kihara,§ Takaaki Nishimoto,§ Hachiro Sugimoto,§ Ryosuke Takahashi,* Bradley T. Hyman,† Shun Shimohama,¶ Oksana Berezovska† and Ayae Kinoshita‡

*Department of Neurology, Graduate School of Medicine, Kyoto University, Kyoto, Japan
†Alzheimer Research Unit, Massachusetts General Hospital, Charlestown, Massachusetts, USA
‡School of Health Sciences, Graduate School of Medicine, Kyoto University, Kyoto, Japan
§Department of Neuroscience for Drug Discovery, Graduate School of Pharmaceutical Sciences, Kyoto University, Kyoto, Japan
¶Department of Neurology, Sapporo Medical University, Sapporo, Japan

Abstract

In neurons, Presenilin 1(PS1)/γ-secretase is located at the synapses, bound to N-cadherin. We have previously reported that N-cadherin-mediated cell–cell contact promotes cell-surface expression of PS1/γ-secretase. We postulated that N-cadherin-mediated trafficking of PS1 might impact synaptic PS1-amyloid precursor protein interactions and Aβ generation. In the present report, we evaluate the effect of N-cadherin-based contacts on Aβ production. We demonstrate that stable expression of N-cadherin in Chinese hamster ovary cells, expressing the Swedish mutant of human amyloid precursor protein leads to enhanced secretion of Aβ in the medium. Moreover, N-cadherin expression decreased $A\beta_{42/40}$ ratio. The effect of N-cadherin expression on Aβ production was accompanied by the enhanced accessibility of PS1/γ-secretase to amyloid precursor protein as well as a conformational change of PS1, as demonstrated by the fluorescence lifetime imaging technique. These results indicate that N-cadherin-mediated synaptic adhesion may modulate Aβ secretion as well as the $A\beta_{42/40}$ ratio via PS1/N-cadherin interactions.

Keywords: Alzheimer's disease, amyloid β, N-cadherin, presenilin 1, synapse.

J. Neurochem. (2009) **108**, 350–360.

Amyloid β (Aβ) peptides are the major components of senile plaques, a pathological hallmark of Alzheimer's disease (AD), and are generated by the intramembranous cleavage of the amyloid precursor protein (APP) C-terminal fragment by Presenilin1 (PS1)/γ-secretase (De Strooper *et al.* 1998). PS1 is a multitransmembrane protein with a 30-kDa N-terminal fragment (NT), a 20-kDa C-terminal fragment (CT) and a large cytoplasmic loop domain (Thinakaran *et al.* 1996). Most of the PS1 mutations associated with familial AD (FAD) are known to increase the ratio of $A\beta_{42}$–$A\beta_{40}$ ($A\beta_{42/40}$ ratio), thereby increasing the more aggregation-prone $A\beta_{42}$ relative to $A\beta_{40}$ (Citron *et al.* 1997), which is considered at present to be an important molecular background of FAD pathogenesis. Using fluorescence lifetime imaging microscopy (FLIM), we have previously demonstrated that FAD-linked mutations in PS1 change the spatial relationship between PS1 NT and CT, increasing proximity of the two epitopes (Berezovska *et al.* 2005). This effect was contrary to that observed after the treatment with $A\beta_{42}$-lowering non-steroidal anti-inflammatory drugs (NSAIDs) which leads to the opposite conformational effect with PS1 NT and CT further apart (Lleo *et al.* 2004). These findings suggested that

Received June 20, 2008; revised manuscript received September 10, 2008; accepted October 20, 2008.

Address correspondence and reprint requests to Ayae Kinoshita, School of Health Sciences, Graduate School of Medicine, Kyoto University, 53 Shogoinkawahara-cho, Sakyo-ku, Kyoto 606–8507, Japan. E-mail: akinoshita@hs.med.kyoto-u.ac.jp

Abbreviations used: AD, Alzheimer's disease; APP, amyloid precursor protein; APPSw, APP Swedish mutant; Aβ, amyloid β; CHO, Chinese hamster ovary; CT, C-terminal fragment; FAD, familial AD; FLIM, fluorescence lifetime imaging technique; FRET, fluorescence resonance energy transfer; NSAIDS, nonsteroidal anti-inflammatory drugs; NT, N-terminal fragment; PS1, presenilin 1.

conformational change in PS1 because of mutations or to allosteric influences provides a possible structural basis for altered $A\beta_{42/40}$ ratio.

In neurons, PS1 binds to β-catenin and N-cadherin at the synapse (Georgakopoulos *et al.* 1999). N-cadherin is essential for forming synaptic contact as well as for specific neuronal function such as synaptic plasticity (Bozdagi *et al.* 2000; Togashi *et al.* 2002). Accumulating evidence suggests that Aβ release may be regulated by synaptic activity (Kamenetz *et al.* 2003; Cirrito *et al.* 2005; Lesne *et al.* 2005). However, it remains largely unknown how PS1/γ-secretase-mediated APP cleavage is regulated by synaptic activity. We have recently demonstrated that N-cadherin promotes the cell-surface expression of PS1/γ-secretase via direct interaction with PS1 loop domain (Uemura *et al.* 2007). This result indicated that N-cadherin may recruit PS1/γ-secretase to synaptic sites. Thus, we hypothesize that N-cadherin-based synaptic adhesion may influence Aβ production.

Here, we demonstrate that stable expression of N-cadherin in cadherin-deficient Chinese hamster ovary (CHO) cells expressing human APP Swedish mutant (APPSw) enhances the Aβ levels in the medium, possibly by increasing the accessibility of APP to PS1/γ-secretase. Moreover, N-cadherin expression induces a structural change in PS1, similar to that previously observed to accompany NSAID-induced decrease in $A\beta_{42/40}$ ratio. These results indicate that N-cadherin-PS1 interactions may modulate Aβ production at the synapse, providing novel insight into AD pathophysiology.

Materials and methods

Plasmid constructs

The construction of the expression vector encoding human N-cadherin tagged with HA at its C-terminus was described previously (Uemura *et al.* 2006b). The construction of the plasmid, expressing wtPS1 and the production of deletion mutant of PS1 (Δ340-350PS1), which is unable to interact with N-cadherin was described previously (Uemura *et al.* 2007). Precise cloning of all reading frame was verified by sequencing. The expression vector of APP-GFP was described elsewhere (Kinoshita *et al.* 2002). The original PS1-GFP (in the loop) construct was a generous gift from Dr. Kaether (Ludwig-Maximilians University, Germany) and was created by introducing a NotI-GFP-NotI between codon 351 and 352 of the cytoplasmic loop of human PS1. The RFP fragment with NotI restriction sites at 5′ and 3′ ends was generated by PCR and GFP was replaced by RFP.

Cell culture and transfection

Chinese hamster ovary cells were maintained in Dulbecco's modified Eagle's medium/F12 (Invitrogen, Carlsbad, CA, USA) supplemented with 10% fetal bovine serum. Transient transfection of wtPS1, PS1 mutant (Δ340-350PS1) and N-cadherin into cells were achieved by lipofection method, using Lipofectamine 2000 (Invitrogen) according to the manufacturer's instructions. CHO cells, stably expressing Swedish (K670/M671->N/L) mutant human APP695 (APPSw-CHO cells) and CHO cells stably expressing both Swedish mutant APP and human N-cadherin (APPSw/Ncad-CHO cells) were obtained as described elsewhere (Uemura *et al.* 2007). Primary cultured neurons were obtained from the hippocampus of fetal rats (17–19 days gestation) as described previously (Uemura *et al.* 2006a). Cultures were incubated in Eagle's Minimum Essential Medium supplemented with 10% fetal calf serum or 10% horse serum.

Antibodies and chemical reagents

Mouse monoclonal anti-N-cadherin C-terminus and anti-β-catenin antibodies are obtained from Transduction Laboratories. Mouse monoclonal anti-β-actin antibody, mouse monoclonal anti-N-cadherin N-terminus antibody (N-cadherin neutralizing antibody, GC-4), rabbit polyclonal anti-nicastrin antibody, rabbit polyclonal anti-APP C-terminus antibody and control normal mouse IgG are from Sigma (St Louis, MO, USA). Rabbit polyclonal anti-PS1 N-terminal fragment and control normal rabbit IgG were from Santa Cruz, Santa Cruz, CA, USA. Rabbit polyclonal anti-BACE1 antibody was from Calbiochem, San Diego, CA, USA. Rat monoclonal anti-PS1 N-terminal fragment antibody was from Chemicon, Temecula, CA, USA. Alexa Fluor 546 goat anti-mouse IgG, Alexa Fluor 546-phalloidin, and Alexa Fluor 488 goat anti-rabbit IgG, and Cy3-anti-rabbit IgG were obtained from Molecular Probes, Eugene, OR, USA. Anti-mouse and rabbit horseradish peroxidase-conjugated secondary antibodies are from Amersham Biosciences, Piscataway, NJ, USA.

Cell treatment by reagents

For the inhibition of N-cadherin-mediated cell–cell contact, cells were treated with 80 μg/mL of N-cadherin-neutralizing antibody (GC-4) in OPTI-MEM for indicated period of time. Control cells were treated with an equal amount of normal mouse IgG.

Western blot and immunoprecipitation

Preparation of protein samples, the western blot and immunoprecipitation analysis were carried out as described elsewhere (Uemura *et al.* 2007).

Immunostaining

The samples for immunostaining were prepared as described elsewhere (Uemura *et al.* 2007). After fixation, samples were examined using a laser scanning confocal microscopy, LSM 510 META (Zeiss, Jena, Germany) or BZ-9000 fluorescent microscopy (KEYENCE).

Measurement of BACE1 activity

β-secretase activity was measured by using β-secretase activity kit (R&D systems). Briefly, 2.5×10^5 cells of APPSw-CHO cells or APPSw/Ncad-CHO cells were plated in 3.5 cm dish and cultured overnight. Cells were collected and lysed by adding 500 μL of 1× cell extraction buffer. Protein concentration of each cell lysate was determined by the Bradford method (Uemura *et al.* 2003) and equal amount of protein was subjected to the β-secretase activity assay, according to the manufacturer's instruction.

Fluorescence lifetime imaging microscopy assay

To analyze the PS1 conformation and/or PS1-APP interactions in intact cells expressing or not expressing N-cadherin, the APPSw-

CHO or APPSw/Ncad-CHO cells were fixed and double-immunostained with corresponding antibodies labeled with Cy3 and Alexa 488 for the FLIM analysis. To monitor PS1 conformation, we used goat anti-PS1 NT and rabbit anti-PS1 CT antibodies from Sigma. For the analysis of PS1-APP interactions we used mouse anti-PS1 antibody raised against amino acids 267–378 in the major TM6-7 loop domain (Chemicon) and an antibody to APP CT (Sigma). The fluorescence lifetime of a donor fluorophore (Alexa 488) was measured as described previously (Berezovska *et al.* 2005). In order to confirm the N-cadherin-mediated cell adhesion effect on Aβ production, we also examined the proximity between APP and PS1 in the presence of N-cadherin-neutralizing antibody (GC-4). For this blocking experiment, we modified the protocol for the FLIM assay since GC-4 is a mouse monoclonal antibody, which might cross-react the immunohistochemical results described above. We did two complementary FLIM experiments: (i) CHO cells stably expressing APPSw and N-cadherin were treated for 6 h with 80 μg/mL of either anti-N-cadherin blocking antibody (GC-4) or normal IgG as a control. The cells were fixed and immunostained with antibodies against APP (rabbit anti-APP CT, Sigma) and PS1 (goat anti-PS1 NT, Sigma) for the FLIM analysis. (ii) The cells were transfected with C-terminally labeled APP-GFP and PS1-RFP (tagged in the TM6-7 loop region), treated with CG4 or IgG and the FLIM analysis was performed on the living cells.

Measurement of extracellular Aβ

Aβ peptides produced by rat hippocampus primary neurons were measured by using Mouse/Rat Amyloid β (1–40) (N) Assay Kit (IBL, Gumma, Japan). Primary neurons, cultured in 3.5 cm dish were washed once with OPTI-MEM and then incubated in OPTI-MEM for indicated periods of time. After incubation, the culture medium was collected, centrifugated at 600 *g* for 5 min, and the 100 μL of the aliquot was used for the extracellular sample. $A\beta_{40}$ and $A\beta_{42}$ peptides produced by APPSw-CHO cells or APPSw/Ncad-CHO cells were measured by using Human β Amyloid (1–40) and (1–42) ELIZA Kit (WAKO, Osaka, Japan), respectively. 6×10^5 of APPSw-CHO cells or APPSw/Ncad-CHO cells cultured in 3.5 cm dish were washed once with OPTI-MEM and then incubated in OPTI-MEM for indicated period of time. After incubation, the culture medium was collected, centrifugated 600 *g*, 5 min, and the 100 μL of the aliquot was used for measurement of extracellular Aβ.

Statistical analysis

All values are given in means ± SE Comparisons were performed using a paired Student's *t*-test. For comparison of multiparametric analysis, one-way factorial ANOVA, followed by the *post hoc* analysis by Fisher's PLSD was used. $p < 0.05$ was considered to indicate a significant difference. $n = 4$ indicates four independent experiments.

Results

N-cadherin expression enhances Aβ secretion and reduces $A\beta_{42/40}$ ratio

The purpose of our study is to define the effect of a synaptic adhesion molecule, N-cadherin, on Aβ production by using biochemical (western blot and ELISA) and fluorescence resonance energy transfer (FRET)-based FLIM assay. First, we determined whether stable expression of N-cadherin could enhance the production of Aβ. To test this, CHO cells stably expressing Swedish (K670N/M671L) mutant human APP695 (APPSw-CHO cells) and CHO cells stably expressing both APPSw and human N-cadherin (APPSw/Ncad-CHO cells) were established. The expression levels of BACE1 and γ-secretase components were similar between APPSw-CHO and APPSw/Ncad-CHO cells (Fig. 1a). BACE1 activity was not significantly different between these cell lines (Figure 1b). Immunocytochemical analysis using anti-N-cadherin and anti-PS1 antibodies revealed co-localization of these proteins at the sites of cell–cell contact and at the cell surface [Fig. 1c–f, see also Uemura *et al.* (2007)], indicating that PS1/γ-secretase was recruited to the cell-surface upon formation of N-cadherin-based cell-cell contact.

Next, we compared the levels of $A\beta_{40}$ and $A\beta_{42}$ in the medium between APPSw-CHO and APPSw/Ncad-CHO cells. Both $A\beta_{40}$ (Fig. 2a) and $A\beta_{42}$ (Fig. 2b) levels were increased by stable expression of N-cadherin. Interestingly, the $A\beta_{42/40}$ ratio was significantly reduced in N-cadherin expressing cells (Fig. 2c). We established four independent clones of APPSw/Ncad-CHO cells, all of which produced significantly higher amounts of extracellular $A\beta_{40}$, compared with the original APPSw-CHO cells (Fig. 2d). Moreover, in order to confirm that enhanced Aβ secretion in APPSw/Ncad-CHO cells is specifically caused by the expression of N-cadherin, we used well-characterized N-cadherin-neutralizing antibody (GC-4) (De Wever *et al.* 2004) to inhibit N-cadherin-mediated contacts. The N-cadherin-neutralizing antibody inhibited the release of $A\beta_{40}$ from APPSw/Ncad-CHO cells (Fig. 2e, white columns), whereas it had no effect on APPSw-CHO cells (Fig. 2e, black columns). The level of $A\beta_{40}$ secreted from APPSw/Ncad-CHO cells after N-cadherin-neutralizing antibody treatment was similar to that of the original APPSw-CHO cells, indicating that the enhanced extracellular release of Aβ from these cells was specifically caused by the N-cadherin expression. Next, to confirm the effect of N-cadherin expression on the metabolism of wild-type APP, we established CHO cell line, which expresses wild-type APP with (APPWt/Ncad-CHO cells) or without (APPWt-CHO cells) N-cadherin (Supporting informationFig. S1a). Both stable and transient expression of N-cadherin reduced $A\beta_{42/40}$ ratio in the background of wild-type APP expression. Thus, these results strongly suggest that N-cadherin influences wild-type as well as mutant APP metabolism (Supporting information Figure S1b–e).

N-cadherin expression increases the accessibility of PS1/γ-secretase to its substrate APP

We have previously demonstrated by the FLIM assay that close association of PS1 and APP preferentially occurs in the

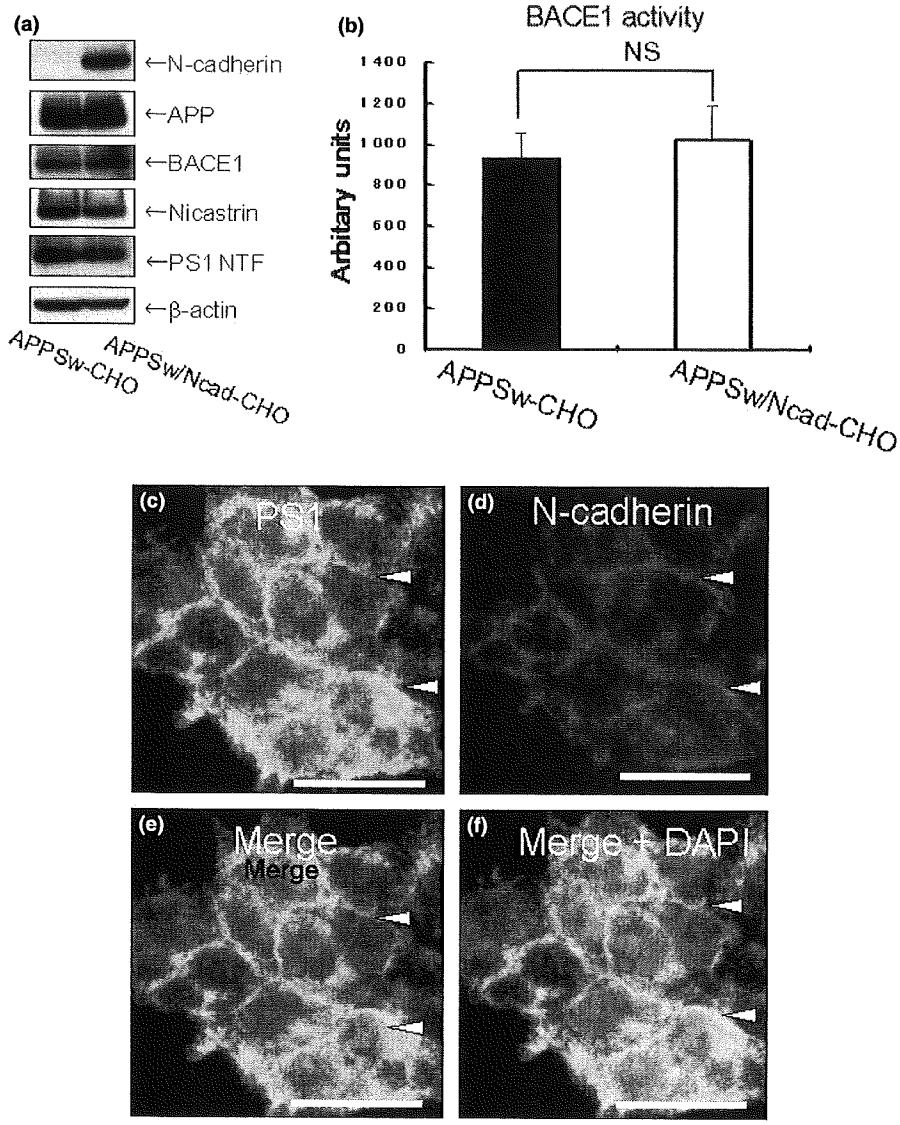

Fig. 1 Characterization of APPSw/Ncad-CHO cells. (a) APPSw-CHO cells and APPSw/Ncad-CHO cells were analyzed by western blot. N-cadherin was expressed only in APPSw/Ncad-CHO cells. The expression levels of APP, BACE1, nicastrin, PS1 NT were similar in both cell lines. The bottom lane indicates the β-actin level, which was used as a loading control. (b) APPSw-CHO cells and APPSw/Ncad-CHO cells were lysed and β-secretase activity in the lysate was measured. No significant difference was found between these cell lines ($p = 0.15$, $n = 4$). (c–f) APPSw/Ncad-CHO cells were immunostained with with rabbit polyclonal anti-PS1 NT (c) and mouse monoclonal anti-N-cadherin antibodies (d). Merged image is shown in (e). Merged image with nuclear DAPI staining is shown in (f). The fixed samples were analyzed by BZ-9000 fluorescent microscopy (KEYENCE). N-cadherin (d) and PS1 (c) immunoreactivities are co-localized at the cell-cell contact sites (arrowheads). Scale bar: 20 μm.

distal subcellular compartments (Berezovska *et al.* 2003). In addition, we have shown that N-cadherin/PS1 interaction changes subcellular distribution of the PS1/γ-secretase, thereby enhancing its expression at the cell-surface (Uemura *et al.* 2007). Thus, we postulated that enhanced secretion of Aβ in N-cadherin expressing cells may be attributed to better accessibility of APP to PS1/γ-secretase. To test this hypothesis we used an established FLIM assay to monitor APP-PS1 interactions (Berezovska *et al.* 2003). PS1 was immunostained with an anti-PS1 loop region antibody labeled with Alexa 488 (FRET donor) and the APP CT was immunostained with a Cy3-labeled antibody (FRET acceptor). The fluorescence lifetime of the Alexa488 donor fluorophore shortens in close vicinity (< 10 nm) of a FRET acceptor fluorophore. The degree of the lifetime shortening is a quantitative measure of proximity. The donor fluorophore

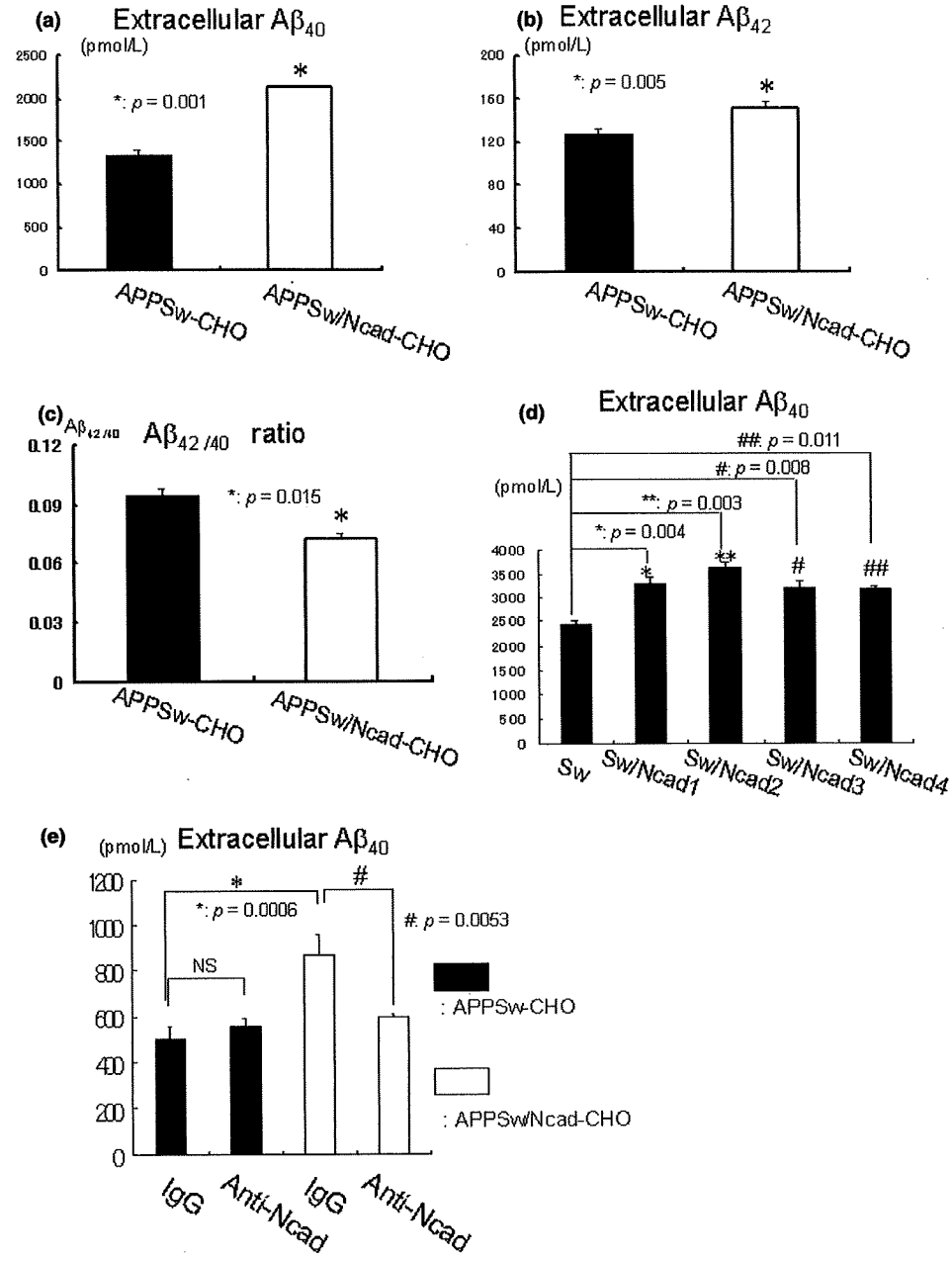

Fig. 2 N-cadherin expression enhances extracellular Aβ levels and reduces $A\beta_{42/40}$ ratio. (a) APPSw-CHO cells or APPSw/Ncad-CHO cells were incubated in OPTI-MEM for 12 h. The amount of extracellular $A\beta_{40}$ was significantly elevated in APPSw/Ncad-CHO cells, compared with APPSw-CHO cells ($n = 8$, $^*p = 0.001$). (b) APPSw-CHO cells or APPSw/Ncad-CHO cells were incubated in OPTI-MEM for 12 h. After incubation, culture medium was collected and the amount of extracellular $A\beta_{42}$ was measured. Extracellular $A\beta_{42}$ was significantly elevated in APPSw/Ncad-CHO cells, compared with APPSw-CHO cells ($n = 8$, $^*p = 0.005$). (c) The $A\beta_{42/40}$ ratio in the medium was significantly decreased in APPSw/Ncad-CHO cells, compared with APPSw-CHO cells ($n = 8$, $^*p = 0.015$). (d) APPSw-CHO (Sw) cells or four independent stable cell lines of APPSw/Ncad-CHO cells (SwNcad1-4) were incubated in OPTI-MEM for 24 h. After incubation, the amount of extracellular $A\beta_{40}$ was measured. Secreted extracellular $A\beta_{40}$ was significantly elevated in every APPSw/Ncad-CHO stable cell line (SwNcad1-4), compared with that in APPSw-CHO cells (Sw) ($n = 4$, $^*p = 0.004$, $^{**}p = 0.003$, $\#p = 0.003$, $\#\#p = 0.011$). (e) APPSw-CHO cells or APPSw/Ncad-CHO cells were incubated in fresh OPTI-MEM containing either control IgG or N-cadherin-neutralizing antibody for 6 h. After incubation, the amount of extracellular $A\beta_{40}$ was measured. N-cadherin-neutralizing antibody significantly reduced the extracellular $A\beta_{40}$ release into the medium in APPSw/Ncad-CHO cells ($^*p = 0.006$, $n = 4$). Conversely, N-cadherin-neutralizing antibody had no effect on the extracellular $A\beta_{40}$ release into the medium in APPSw -CHO cells ($\#p = 0.0053$, $n = 4$).

Table 1 FRET between PS1 loop and APP CT in CHOSw compared with NcadCHOSw cells

Cell line	FRET donor (Alexa 488)	FRET acceptor (Cy3)	Alexa 488 lifetime in ps (mean ± SE)	*p* value (compared with CHOSw PS1 loop APP CT)
APPSw-CHO (n = 10)	PS1 loop	None (negative control)	1932 ± 7	$p < 0.0001$
APPSw-CHO (n = 10)	PS1 loop	APP CT	1790 ± 22	
APPSw/Ncad-CHO (n = 12)	PS1 loop	APP CT	1644 ± 25	$p < 0.0001$

lifetime can be color-coded and displayed on a pixel-by-pixel basis through the entire image of the cell: if APP and PS1 molecules are closer together, the donor fluorescence lifetime will be shorter, and the color will be closer to red. The FLIM analysis showed that Alexa 488 lifetime was significantly shortened in APPSw/Ncad-CHO cells, compared with that in APPSw-CHO cells, indicating that PS1 and APP came into closer proximity (or increased percentage of molecules are in close proximity to one another) in the presence of N-cadherin (Table 1). Pseudocolor FLIM image showed more red pixels per cell (i.e., more interacting molecules per cell) in APPSw/Ncad-CHO cells (Fig. 3b), compared with that in APPSw-CHO cells (Fig. 3a). This indicates that N-cadherin expression may increase the accessibility of PS1/γ-secretase to its substrate APP. In order to examine the effect of N-cadherin-mediated cell adhesion on APP/PS1 interaction, we also examined the proximity of APP and PS1 in the presence of N-cadherin-neutralizing antibody (GC-4). We performed two complementary FLIM experiments; one with immunohistochemistry using goat anti-PS-NT antibody and rabbit anti-APP-CT antibody (Table 2) and the other using live cells expressing APP-GFP and PS1-RFP (Table 3), in the presence of either GC-4 or normal mouse IgG as a control. In both blocking experiments, we observed significantly longer donor fluorophore lifetime in GC4 treated cells, comparing with that in IgG- treated cells, indicating that N-cadherin-based cell-cell adhesion specifically modulates the accessibility of APP to PS1/γ-secretase. To confirm these results biochemically, we transfected N-cadherin into HEK293 cells and analyzed whether N-cadherin expression enhances the APP-PS1 interaction by immunoprecipitation. As expected, APP-PS1 interaction was increased in N-cadherin expressing cells (Supporting information Fig. S2), indicating that N-cadherin expression brings APP and PS1/γ-secretase in closer proximity.

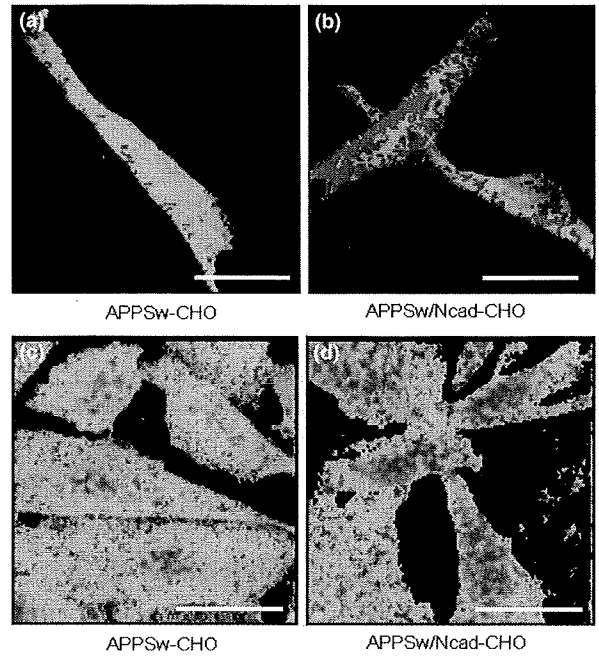

Fig. 3 N-cadherin expression in CHO cells increases PS1-APP interactions and induces conformational change of PS1/γ-secretase. (a and b) For the FLIM assay, PS1 is stained at its loop region with Alexa 488 (FRET donor) and APP is stained at its CT with Cy3(FRET acceptor). The fluorescence lifetime of Alexa 488 is displayed as a pseudocolor image: if PS1 and APP molecules are closer together, the donor fluorescence lifetime will be shorter, and the color will be closer to red. Alexa488 lifetime was significantly shortened in APPSw/Ncad-CHO cells (b), compared with that in APPSw-CHO cells (a), indicating that PS1 and APP came into closer proximity in the presence of N-cadherin. Scale bar: 10 μm. (c and d) APPSw-CHO (c) or APPSw/Ncad-CHO (d) cells were immunostained with antibodies against PS1 NT (Alexa 488) and CT (Cy3). The proximity between PS1 NT and CT was evaluated by measuring lifetime of the Alexa 488 donor fluorophore (PS1 NT Alexa 488) in the FLIM assay. The fluorescence lifetime of Alexa 488 is displayed as a pseudocolor image. Red pixels indicate close proximity between PS1 N- and C-termini. Alexa 488 lifetime in APPSw/Ncad-CHO (d) cells was significantly increased, compared with that in APPSw-CHO cells (c), indicating that N-cadherin 'opened' PS1 conformation with NT and CT further apart. Scale bar: 10 μm.

N-cadherin expression induces the conformational change of PS1

Whereas total Aβ was increased in N-cadherin expressing cells, the $A\beta_{42/40}$ ratio was reduced (Fig. 2c). We and others have demonstrated previously that $A\beta_{42/40}$ ratio correlates with PS1 conformation in intact cells: familial Alzheimer's disease mutations in PS1 that elevate $A\beta_{42/40}$ ratio decreased (Berezovska *et al.* 2005), while $A\beta_{42}$-lowering NSAIDs (Lleo *et al.* 2004) or structural changes in γ-secretase component, Pen2 (Isoo *et al.* 2007) increased, PS1 NT-CT proximity. Therefore, we investigated whether change in $A\beta_{42/40}$ ratio observed in cells

Table 2 FRET between PS1 N-terminus and APP CT in NcadCHOSw cells treated with N-cadherin neutralizing GC-4 antibody or IgG as a control

Cell line	FRET donor (Alexa 488)	FRET acceptor (Cy3)	Alexa 488 lifetime in ps (mean ± SE)	*p* value (compared with control IgG)
NcadCHOSw (Negative Control)	PS1 NT	None	1903 ± 28	$p < 0.01$
NcadCHOSw with control IgG ($n = 21$)	PS1 NT	APP CT	1677 ± 22	
NcadCHOSw with GC-4 ($n = 17$)	PS1 NT	APP CT	1789 ± 100	

Table 3 FRET between PS1 loop and APP CT in living NcadCHOSw cells treated with GC-4 or IgG

Cell line	FRET donor	FRET acceptor	Alexa 488 lifetime in ps (mean ± SE)	*p* value (compared with control IgG)
NcadCHOSw (Negative Control)	APP-GFP	None	2076 ± 62	$p < 0.01$
NcadCHOSw with control IgG ($n = 21$)	APP-GFP	PS1-RFP(loop)	1646 ± 223	
NcadCHOSw with GC-4 ($n = 17$)	APP-GFP	PS1-RFP(loop)	1859 ± 74	

with tighter cell-cell adhesion mediated by N-cadherin is due to a conformational change in PS1/γ-secretase. The proximity between PS1 NT and CT in fixed and detergent permeabilized cells was evaluated by measuring lifetime of the Alexa 488 donor fluorophore (PS1 NT Alexa 488) in the absence (negative control) and presence of the Cy3 acceptor on the PS1 CT. As expected, the Alexa 488 donor fluorophore lifetime shortened when the PS1 CT was labeled with the Cy3 acceptor (Table 4), consistent with the close proximity between the PS1 NT and CT in APPSw-CHO cells. In contrast, Alexa 488 lifetime in APPSw/Ncad-CHO cells was significantly longer (1821 + −14 ps), compared with that in APPSw-CHO cells, indicating that N-cadherin 'opened' the PS1 conformation with NT and CT being further apart (Tables 2 and 3, Fig. 3c and d). Thus, these results are in agreement with the previous findings that more 'open' PS1 conformation correlates with generation of the shorter Aβ species (Lleo *et al.* 2004), and therefore decreased $A\beta_{42/40}$ ratio in APPSw/Ncad-CHO cells may be attributed to the change in conformation of the PS1/γ-secretase due to N-cadherin over-expression.

PS1/N-cadherin interaction affects both Aβ production and $A\beta_{42/40}$ ratio

Since N-cadherin interacts with the cytoplasmic loop of PS1 CTF (Georgakopoulos *et al.* 1999), we next determined whether the PS1/N-cadherin interaction affects Aβ production and/or $A\beta_{42/40}$ ratio. To test this, either wtPS1 or a PS1 mutant lacking the N-cadherin interaction domain [Δ340-350PS1, Uemura *et al.* 2007] was transfected into APPSw/Ncad-CHO cells. Since PS1/γ-secretase acts in a complex including PS1, Nicastrin, Pen-2 and Aph-1 (Takasugi *et al.* 2003), Δ340-350PS1 competes with endogenous wild-type PS1 to occupy other components of γ-secretase and act in a dominant-negative fashion (Thinakaran *et al.* 1997). As expected, immunoprecipitation assay revealed that Δ340-350PS1 does not interact with N-cadherin (Fig. 4a). We found that the extracellular levels of both $A\beta_{40}$ (Fig. 4b) and $A\beta_{42}$ (Fig. 4c) were decreased after the transient expression of Δ340-350PS1, compared with wtPS1. In addition, $A\beta_{42/40}$ ratio in the medium was increased in the Δ340-350PS1 transfectants, compared with that in wtPS1 (Fig. 4d), indicating that the PS1/N-cadherin interaction affects both Aβ production and $A\beta_{42/40}$ ratio.

Discussion

In this report, we demonstrate that introducing N-cadherin into cadherin-deficient CHO cells increased secreted $A\beta_{40}$ and $A\beta_{42}$ levels (Fig. 2). The expression of N-cadherin in CHO cells elevates cell-surface levels of PS1/γ-secretase [Uemura *et al.* 2007], see also Fig. 1. Thus, the effect of

Table 4 FRET between PS1 NT and CT in CHOSw compared with NcadCHOSw cells

Cell line	FRET donor (Alexa 488)	FRET acceptor (Cy3)	Alexa 488 lifetime in ps (mean ± SE)	*p* value (compared with NcadCHOSw)
APPSw-CHO ($n = 11$)	PS1 NT	None (negative control)	1897 ± 7	$p < 0.0001$
APPSw-CHO ($n = 14$)	PS1 NT	PS1 CT	1524 ± 46	$p = 0.0002$
APPSw/Ncad-CHO ($n = 14$)	PS1 NT	PS1 CT	1821 ± 14	

